Conservative finite difference time domain schemes for the prestressed Timoshenko, shear and Euler–Bernoulli beam equations

Conservative Finite Difference Time Domain Schemes for the Prestressed Timoshenko, shear and Euler-Bernoulli Beam Equations.

Michele Ducceschi and Stefan Bilbao

Acoustics and Audio Group,
James Clerk Maxwell Building,
University of Edinburgh,
EH9 3JZ, Edinburgh UK

Abstract

This paper presents a number of finite difference time domain (FDTD) schemes to simulate the vibration of prestressed beams to various degrees of accuracy. The Timoshenko, shear and Euler-Bernoulli models are investigated, with a focus on the numerical modelling for the Timoshenko system. The conservation of a discrete Hamiltonian to machine accuracy ensures stability and convergence of the numerical schemes. The difference equations are in the form of theta schemes, which depend on a number of free parameters that can be tuned in order to reduce numerical dispersion. Although the schemes are built by means of second-order accurate finite difference operators only, fully fourth-order accurate schemes may be designed through modified equation techniques, and wideband-accurate schemes are also possible. The latter are schemes designed to maximise the resolving power at all wavelengths. Investigation of beams of cross section varying from from slender to thick allows a thorough comparison between the various schemes, for the three beam models.

Keywords: Prestressed Beams, Timoshenko Beam, Stiff strings, Numerical Methods

1. Introduction

The vibration of beams is a topic of longstanding and continuing interest for obvious reasons: beams are among the most common engineering elements found in a variety of machines, and serve as main structural elements in buildings, bridges and railroads [1, 2]. Though, through finite element analysis [3], it is possible to simulate 3D beam dynamics resulting from elasticity theory and appropriate constitutive laws, approximate theories remain a popular choice in the numerical setting, due primarily to reduced computational cost and ease of implementation. In such theories, the 3D formulation is reduced to a 1D problem expressed as a system of partial differential equations (PDEs). Three such 1D beam theories are commonly seen in the literature. In ascending order of complexity, these are known as the Euler-Bernoulli model, the shear model and the Timoshenko model [4, 5]. The Timoshenko beam theory (the main subject of this paper) models both flexural and shear waves, and is an excellent approximation to full 3D theories over a large range of beam thicknesses [1]. The Timoshenko model results in two distinct dispersion curves and, at high frequencies, its spectrum is driven by shear motion as well as flexural. At low frequencies, for thin beams, the three models yield similar modal frequencies and shapes [6].

With regard to numerical simulation, various methods have been proposed for the simulation of the Timoshenko beam equations. These range from the finite element methods mentioned above [7, 8, 9, 10, 11, 12, 13, 14, 15], to reduced-order methods (Galerkin [16] and modal methods [17]),

to pseudospectral methods [18] and specialised methods such as Discrete Singular Convolution [19]. Most of the work cited above deals with the problem of calculating the first few eigenfrequencies of the Timoshenko system, for engineering purposes. On the other hand, full time domain simulation has not seen much investigation. Notable exceptions are represented by the work of Sarigül and Aksu [20], Li and Sun [21] and Almeida Junior [22] using finite difference schemes and by the work of Chabassier *et. al* [23, 24]. The latter is an interesting application of the Timoshenko beam theory used to model a vibrating piano string. In this work, the focus will be on the development of stable and consistent finite difference schemes. The accuracy of the schemes can be increased from the natural second-order accuracy originating from the application of second-order accurate finite difference operators, by means of a number of free parameters. These ideas are borrowed from the literature on the modified equation methods that first appeared on the study of the wave equation, see for instance [25, 26, 27, 28, 29]. Two cases of interest will be presented: fourth-order accurate and wideband accurate schemes. The latter are especially useful when good resolution at all wavelengths is needed, for a fixed time step or grid spacing, although the formal order of accuracy in time and space remains 2 [30].

The paper is structured as follows: Section 2 is an overview of the Timoshenko beam theory, useful in order to discuss the properties of the numerical schemes in section 3. Important aspects related to numerical dispersion and the modal distribution will be discussed with regard to the choice of an appropriate time step. The stability of the schemes is deduced from energy conservation properties. Simulation results are presented in Section 4.

1.1. Case Studies and Physical Parameters

Before introducing the model itself, it is useful to provide physical parameters for particular cases of beams to be considered here. The beams are assumed made of steel, and of circular cross section. The following table contains symbols and corresponding numerical values for the defining parameters of the beam. Three values are given for the beam radius, spanning two orders of magnitude, and corresponding to the three beams considered in this work (thick, medium, thin).

	units	symbol	value
density	$\mathrm{kg/m^3}$	ρ	8000
Young's mod.	Pa	E	$2 \cdot 10^{11}$
Poisson's r.	-	ν	0.30
tension	N	T_0	1000
length	m	L_0	1
radius	m	r	$[10^{-1}, 10^{-2}, 10^{-3}]$

Other auxiliary parameters appear in the Timoshenko beam equations, and can be calculated as follows:

	units	formula	symbol	value
shear mod.	Pa	$E/2(1+\nu)$	G	$7.69 \cdot 10^{10}$
shear coeff.	-	$6(1+\nu)/(7+6\nu)$	κ	0.89
area	$\mathrm{m^2}$	πr^2	A	$\pi \cdot [10^{-2}, 10^{-4}, 10^{-6}]$
m. of inertia	$\mathrm{m^4}$	$\pi r^4/4$	I	$\frac{\pi}{4} \cdot [10^{-4}, 10^{-8}, 10^{-12}]$

2. Timoshenko's Beam Theory

Before describing the numerical scheme at the core of this paper, it is worth recalling some salient aspects of the Timoshenko beam theory. Of prime importance is the presence of two distinct branches in the dispersion relation, yielding, ultimately, two families of modes below and above the cutoff. Central to the construction of a finite difference scheme is the notion of a discrete conserved Hamiltonian, and thus in this section the continuous Hamiltonian will be presented with an eye towards the construction of its discrete counterpart in 3.5.

2.1. Timoshenko's Beam Model

The vibration of a beam under tension may be described by the following system of partial differential equations, known collectively as Timoshenko's beam equations with tension:

$$\rho A\ \partial_t^2 w = T_0\ \partial_x^2 w + A\kappa G \partial_x(\partial_x w - \phi) \tag{1a}$$

$$\rho I\ \partial_t^2 \phi = EI\ \partial_x^2 \phi + A\kappa G(\partial_x w - \phi). \tag{1b}$$

In the system above, $w(x,t)$ and $\phi(x,t)$ represent, respectively, the transverse displacement and shear angle for time $t \geq 0$ and for axial coordinate $x \in \mathcal{D} \triangleq [0, L_0]$, for some length L_0, and where ∂_t and ∂_x represent partial differentiation with respect to t and x.

As a starting point, it is useful to scale the system. To this end, consider the following nondimensional variables denoted by overbars

$$\bar{w} = \frac{w}{w_0}, \quad \bar{\phi} = \frac{\phi}{\phi_0}, \quad \bar{x} = \frac{x}{x_0}, \quad \bar{t} = \frac{t}{t_0}, \quad \bar{L}_0 = \frac{L_0}{x_0}$$

under the following choices of scaling coefficients:

$$x_0^2 = \frac{I}{A}, \quad t_0^2 = \frac{\rho I}{A\kappa G}, \quad \phi_0 = \frac{w_0}{x_0}, \quad \alpha = 1 + \frac{T_0}{A\kappa G}, \quad \beta = \frac{E}{\kappa G}.$$

When rewritten in terms of dimensionless variables (dropping the overbar notation) the Timoshenko system is as follows

$$\partial_t^2 w = \alpha \partial_x^2 w - \partial_x \phi, \tag{2a}$$

$$\partial_t^2 \phi = \beta \partial_x^2 \phi + \partial_x w - \phi. \tag{2b}$$

System (2) requires the specification of two boundary conditions at each end of the domain $\mathcal{D}$. A variety of choices of the boundary conditions have been discussed in detail in [6]. In this article, where the focus is on numerical modeling of the dispersive characterstics of the beam, simply-supported conditions are assumed at the beam ends, i.e.

$$w = \partial_x \phi = 0 \qquad \text{at} \qquad x = 0, L_0. \tag{3}$$

System (2) also requires the specification of w, $\partial_t w$, ϕ and $\partial_t \phi$ at $t = 0$, for $x \in \mathcal{D}$.

2.2. Dispersion Relations

System (2), when examined over the infinite spatial domain $x \in \mathbb{R}$, yields a dispersion relation, obtained under the assumption of monochromatic wavelike solutions of the form

$$\begin{pmatrix} w \\ \phi \end{pmatrix} = \begin{pmatrix} \hat{w} \\ \hat{\phi} \end{pmatrix} e^{j(\omega t + \gamma x)}$$

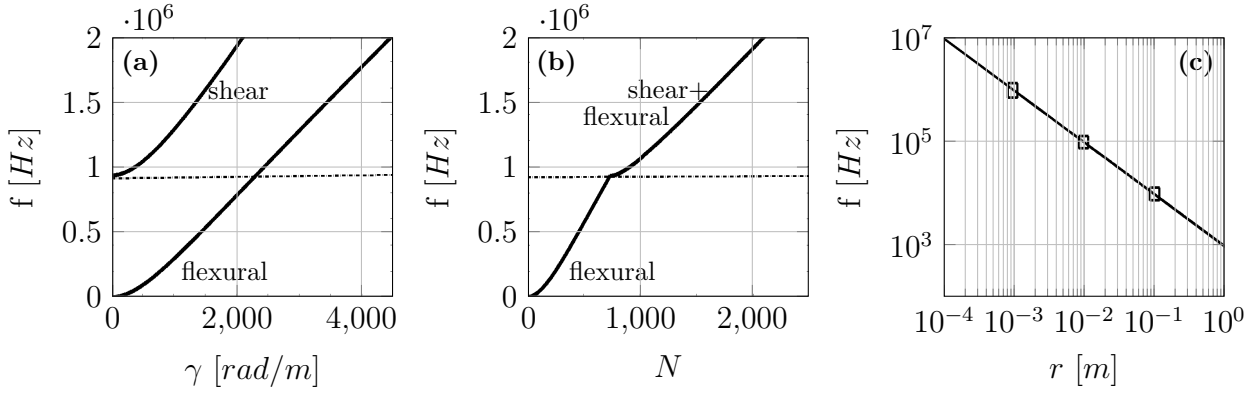

Figure 1: (a): Timoshenko dispersion relation for the small-thickness beam ($r = 0.001$ m). (b): modal distribution. (c): cutoff frequency ω_c as a function of the beam radius; squares indicate the cutoff frequencies for the three beams under study.

for complex amplitudes $\hat{w}, \hat{\phi}$, and for real frequencies and wavenumbers ω, γ.

An characteristic equation in γ, ω results:

$$\omega^4 - \omega^2 - \gamma^2 + \alpha\gamma^2 - \alpha\gamma^2\omega^2 - \beta\gamma^2\omega^2 + \alpha\beta\gamma^4 = 0 \tag{4}$$

The dispersion relation, composed of two branches written here as $\omega_\pm(\gamma)$, follows as

$$\omega_\pm^2 = \frac{(\alpha+\beta)\gamma^2 + 1}{2} \pm \frac{\left(\left(1 + (\beta-\alpha)\,\gamma^2\right)^2 + 4\gamma^2\right)^{1/2}}{2}. \tag{5}$$

Plots of the dispersion relation, for the beam of radius $r = 0.001$ m are shown in Fig. 1(a), where the branches are denoted *flexural* and *shear*. This labelling helps convey the idea that the lower and upper branches correspond mainly to flexural and shear motion, respectively. Notice in particular that the shear branch does not vanish in the limit of $\gamma \to 0$. In fact,

$$\lim_{\gamma\to 0} \omega_+ \triangleq \omega_c = 1 \tag{6}$$

In the notation for ω_c the subscript c indicates the *cutoff*. This implies, in particular, that phase velocities are infinite for these solutions in the limit of low frequencies.

2.3. Modes

The presence of two distinct dispersion relation branches has a consequence on the distribution of the modes. It is possible to define two sets of modes, one below and one above the cutoff frequency ω_c. Consider the following expressions for wavenumber as a function of frequency

$$\gamma_+^2 = \frac{(\beta\omega^2 + \alpha\omega^2 - \alpha + 1) + \left[(\beta\omega^2 + \alpha\omega^2 - \alpha + 1)^2 - 4\alpha\beta(\omega^4 - \omega^2)\right]^{1/2}}{2\alpha\beta}$$

$$\gamma_-^2 = \frac{(\beta\omega^2 + \alpha\omega^2 - \alpha + 1) - \left[(\beta\omega^2 + \alpha\omega^2 - \alpha + 1)^2 - 4\alpha\beta(\omega^4 - \omega^2)\right]^{1/2}}{2\alpha\beta}$$

Below and above the cutoff, the modal frequencies for the simply-supported end conditions (3) are obtained by solving

$$\sin(\gamma_+ L_0) = 0, \qquad \omega \leq \omega_c \tag{7a}$$

$$\sin(\gamma_- L_0)\sin(\gamma_+ L_0) = 0, \qquad \omega > \omega_c. \tag{7b}$$

A picture of the modal distribution is given in Fig.1(b), with the two branches clearly visible. Fig.1(c) shows cutoff frequency as a function of the beam radius. In physical units, the cutoff is given by

$$\omega_c^2 = \frac{A\kappa G}{\rho I} \propto r^{-2} \tag{8}$$

and is thus inversely proportional to the radius. For the thin beam considered here ($r = 1$ mm), the cutoff frequency is $\omega_c = 5.8 \cdot 10^6$ rad/s.

2.4. Hamiltonian

The definition of a non-negative Hamiltonian function associated with (2) is central to the proof of stability for the discrete numerical scheme. A strong solution to the system exists over the domain $x \in \mathcal{D}$ (see for instance Chabassier *et al.* [23]). Hence w, ϕ and their derivatives up to the order 2 necessarily belong to a set $V : \mathcal{D} \times \mathbb{R}^+$ such that, for any function $v(x,t) \in V$, $v(x,t)$ is of class at least $\mathcal{C}^0$ and $v(x,t) \in L^2(\mathcal{D})$. It is then possible to define, for two functions v_1, $v_2 \in V$, the following scalar product and norm

$$\langle v_1, v_2 \rangle \triangleq \int_0^{L_0} v_1 v_2 \, \mathrm{d}x, \quad \|v_1\|^2 \triangleq \langle v_1, v_1 \rangle . \tag{9}$$

Using this notation, the associated Hamiltonian is [6]

$$\mathcal{H} = \frac{\|\partial_t w\|^2}{2} + \frac{\|\partial_t \phi\|^2}{2} + \frac{\beta \|\partial_x \phi\|^2}{2} + \frac{\|\phi - \partial_x w\|^2}{2} + \frac{(\alpha - 1)\|\partial_x w\|^2}{2} \tag{10}$$

The Hamiltonian is composed of kinetic terms (proportional to the squared norms of the velocities) and of potential terms, and is clearly non-negative. Imposing energy conserving end conditions such as (3), a power balance equation may be written as

$$\frac{d}{dt}\mathcal{H} = 0. \tag{11}$$

Under unforced conditions, the power balance is a statement of passivity for the Timoshenko beam equation—in other words there is no spontaneous creation of energy within the system, or at the boundaries.

2.5. Other Engineering Models

It is useful to introduce at this stage the other engineering models. The *shear* model is obtained from the Timoshenko model by neglecting the inertia of the cross section, leading to

$$\partial_t^2 w = \alpha \partial_x^2 w - \partial_x \phi, \tag{12a}$$

$$0 = \beta \partial_x^2 \phi + \partial_x w - \phi. \tag{12b}$$

These equations may be coalesced into a single equation, of second order in time differentiation, as

$$(1 - \beta \partial_x^2)\partial_t^2 w = (\alpha - 1)\partial_x^2 w - \alpha\beta \partial_x^4 w \tag{13}$$

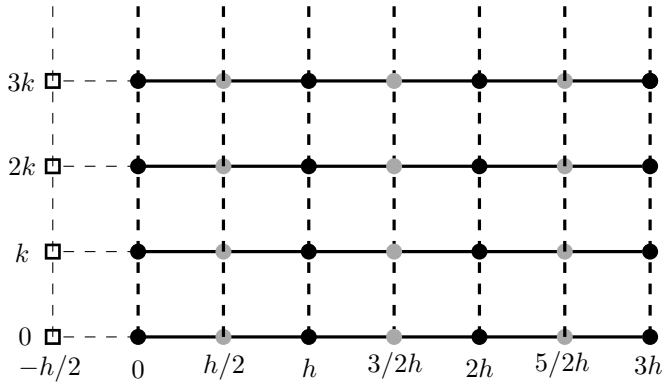

Figure 2: Staggered grids for the grid functions w_m, $\phi_{m+1/2}$, for scheme (15). The ghost point at $-h/2$ (needed for simply supported end conditions) is represented by a square, whereas the actual grid points are drawn as disks. Black disks are the grid points for w_m, grey disks are the grid points for $\phi_{m+1/2}$. The vertical axis is time.

The *Euler-Bernoulli* model is the simplest and perhaps most popular engineering model, and is obtained from (13) in the limit of low wavenumbers. It may be written as

$$\partial_t^2 w = (\alpha - 1)\partial_x^2 w - \beta \partial_x^4 w \tag{14}$$

Both the shear model and the Euler-Bernoulli model possess a conserved, non-negative Hamiltonian; see [6].

3. Finite Difference Schemes

Numerical approximations to the solutions to the Timoshenko system will be developed here using finite difference schemes, which are a natural choice for 1D systems. The particular structure of the Timoshenko system suggests spatially interleaved grid functions. Let w_m^n represent an approximation to $w(x,t)$ at grid locations $x = mh$ and at times $t = nk$, for integer m and n, and where h is the grid spacing and k is the time step. $\phi_{m+1/2}^n$ is defined over a spatially staggered grid, representing an approximation to $\phi(x,t)$ at $x = (m+1/2)h$ and $t = nk$. See Fig. 2.

The grid spacing h is assumed to divide the domain length L_0 evenly, such that $L_0/h = N$ for some integer M. Thus w_m^n is defined for $m = 0, \ldots, M$ and $\phi_{m+1/2}^n$ for $m = 0, \ldots, M-1$.

3.1. Difference Operators And Finite Fifference Schemes

For the grid function w_m^n or the interleaved grid function $\phi_{m+1/2}^n$, the shift operators (in time and space) are defined as in Table 1. Approximations to partial derivatives and the identity may be constructed using these basic operations. Basic such finite difference operators are in given in Table 2. Using the definitions in Tables 1 and 2, three different schemes are now given.

3.2. Second-Order Accurate Scheme

A simple scheme can be obtained immediately by direct substitution of the continuous operators in (2) with the operators given Table 2. The scheme is

$$\delta_{tt} w_m^n = \alpha \delta_{xx} w_m^n - \delta_{x-} \phi_{m+1/2}^n \qquad m = 1 \ldots, M-1 \tag{15a}$$

$$\delta_{tt} \phi_{m+1/2}^n = \beta \delta_{xx} \phi_{m+1/2}^n + \delta_{x+} w_m^n - \phi_{m+1/2}^n \qquad m = 1 \ldots, M \tag{15b}$$

	symbol	definition	
forward time shift	e_{t+}	$e_{t+}w_m^n = w_m^{n+1}$	
backward time shift	e_{t-}	$e_{t-}w_m^n = w_m^{n-1}$	
forward space shift	e_{x+}	$e_{x+}w_m^n = w_{m+1}^n$	$e_{x+}\phi_{m+1/2}^n = \phi_{m+3/2}^n$
backward space shift	e_{x-}	$e_{x-}w_m^n = w_{m-1}^n$	$e_{x-}\phi_{m+1/2}^n = \phi_{m-1/2}^n$

Table 1: Shift operators

Numerical simply-supported conditions can be given as

$$w_0 = 0, \quad \delta_{x-}\phi_{1/2} = 0, \quad w_M = 0, \quad \delta_{x+}\phi_{M-1/2} = 0. \tag{16}$$

Imposing such conditions implies settings for the values of the function $\phi_{m+1/2}$ at the so-called *ghost points* $\phi_{-1/2}$, $\phi_{M+1/2}$. The grid function w_m is zero at the end points, and thus the values at such location need not be stored. Hence, at each time-step the grid functions w_m, $\phi_{m+1/2}$ can be written as arrays of length $M-1$ and M respectively.

3.3. Fourth-Order Accurate Scheme

A fourth-order accurate scheme for the Timoshenko system, employing a finite element method, is given in [23]. Here, a novel scheme, employing only formally second-order accurate finite difference operators, is derived. It is a modification of (15), making use of five free parameters here denoted θ_i, $i = 1, ..., 5$. The scheme is

$$s(\theta_1)\delta_{tt}w_m^n = (\alpha-1)s(\theta_2)\delta_{xx}w_m^n + p(\theta_3)(\delta_{xx}w_m^n - \delta_{x-}\phi_{m+1/2}^n) \qquad m = 1\ldots, M-1 \tag{17a}$$

$$q(\theta_4)\delta_{tt}\phi_{m+1/2}^n = (\beta+1-q(\theta_5))\delta_{xx}\phi_{m+1/2}^n + p(\theta_3)(\delta_{x+}w_m^n - \phi_{m+1/2}^n) \quad m = 1\ldots, M \tag{17b}$$

where

$$s(\theta) \triangleq 1 + \frac{(1-\theta)}{2}h^2\delta_{xx}, \quad p(\theta) \triangleq 1 + \frac{(1-\theta)}{2}k^2\delta_{tt}, \quad q(\theta) \triangleq 1 + \frac{(1-\theta)}{2}h^2 \tag{18}$$

Clearly, this system reduces to (15) under the choice $\theta_i = 1$ for all i, and is consistent with the continuous system when k, h tend to zero. For fourth-order accuracy, the free parameters must be chosen as

$$\theta_1 = \frac{2\alpha^2 + 14\beta\alpha + \beta + 1}{12\alpha\beta} \tag{19a}$$

$$\theta_2 = \frac{\alpha - 6\beta + 8\alpha\beta}{6\alpha\beta - 6\beta} \tag{19b}$$

$$\theta_3 = \frac{10\alpha + \beta + 1}{12\alpha} \tag{19c}$$

$$\theta_4 = \frac{12\alpha\beta - \beta - 1}{12\alpha\beta} \tag{19d}$$

$$\theta_5 = \frac{5\alpha\beta - \beta - 1}{6\alpha\beta} \tag{19e}$$

Fourth-order accuracy is achieved as h, k tend to zero along a path in the h, k space dictated by stability considerations. The order of accuracy is calculated for the dispersion relation, i.e. the

	symbol	definition	Taylor exp.
forward time difference	δ_{t+}	$\dfrac{e_{t+}-1}{k}$	$\dfrac{d}{dt}+O(k)$
backward time difference	δ_{t-}	$\dfrac{1-e_{t-}}{k}$	$\dfrac{d}{dt}+O(k)$
centred time difference	$\delta_{t\cdot}$	$\dfrac{e_{t+}-e_{t-}}{2k}$	$\dfrac{d}{dt}+O(k^2)$
second time difference	δ_{tt}	$\dfrac{e_{t+}-2+e_{t-}}{k^2}$	$\dfrac{d^2}{dt^2}+O(k^2)$
backward time identity	μ_{t-}	$\dfrac{1+e_{t-}}{2}$	$1+O(k)$
second order time identity	μ_{tt}	$\dfrac{e_{t+}+2+e_{t-}}{4}$	$1+O(k^2)$
forward space difference*	δ_{x+}	$\dfrac{e_{x+}-1}{h}$	$\dfrac{d}{dx}+O(h^2)$
backward space difference*	δ_{x-}	$\dfrac{1-e_{x-}}{h}$	$\dfrac{d}{dx}+O(h^2)$
second space difference	δ_{xx}	$\dfrac{e_{x+}-2+e_{x-}}{h^2}$	$\dfrac{d^2}{dx^2}+O(h^2)$

* Acting on an interleaved grid function

Table 2: Time and space difference operators

numerical dispersion relation for scheme (17) is an approximation to (5) to the order of h^4, k^4. This will be proven in the following sections. It will be shown that the eigenfrequencies of scheme (17) also follow the same trend.

Notice that, in (17a), the operator $s(\theta_2)$ acting on $\delta_{xx}w_m^n$ generates an operator of width five in space. Hence, an extra pair of boundary conditions, consitent with (16), must be given. For simply-supported conditions, these are [6]

$$\delta_{xx}w_0 = 0, \quad \delta_{xx}w_M = 0. \tag{20}$$

The set of boundary conditions (16) accompanied by (20) is only second-order accurate: hence, on the grid, the order of accuracy is valid only for beams defined over an infinite domain (equivalently, it is valid for disturbances traveling on the grid before reaching either one of the end points).

3.4. Wideband Accurate Scheme

The simulation of many physical phenomena requires the resolution of a large set of wavelengths. Schemes with a formal order of accuracy, such as (15) and (17), fail at representing smaller wavelengths accurately, for given sample rate and grid spacing. finite difference schemes, though, may be designed so to maximise the resolving power at all scales. Such ideas were introduced by Lele [30] in the context of fluid dynamics, and have been exploited in numerous other fields, including vibroacoustics and musical acoustics [23, 31]. One such scheme for the Timoshenko system is here

given as

$$s(\theta)\delta_{tt}w_m^n = (\alpha-1)\delta_{xx}w_m^n + \mu_{tt}(\delta_{xx}w_m^n - \delta_{x-}\phi_{m+1/2}^n) \tag{21a}$$

$$s(\theta)\delta_{tt}\phi_{m+1/2}^n = \beta\mu_{tt}\delta_{xx}\phi_{m+1/2}^n + \mu_{tt}(\delta_{x+}w_m^n - \phi_{m+1/2}^n) \tag{21b}$$

where $s(\theta)$ is defined in (18), and where

$$\theta = \frac{1}{2} + \frac{(\alpha-1)k^2M^2}{2L_0} \tag{22}$$

where L_0 is the nondimensional beam length, and M is the number of modes (equal to the number of grid points) of frequency below the Nyquist limit, $f_s/2 = 1/2k$.

Notice that this scheme employs just one free parameter, and is thus considerably simpler than (17) in terms of analysis. Simply-supported boundary conditions are again of the form (16).

3.5. Energy Considerations And Stability Conditions

Stability conditions for the schemes are now derived. For the sake of conciseness, the results are here simply stated, but a complete proof can be found in Appendix B. They will follow from energy considerations, as detailed below. The energy analysis allows for incorporation of boundary conditions, thus generalising stability results from von Neumann analysis [32]. The idea is that, as in the continuous case, the conservation of a non-negative discrete function of the state of the finite difference scheme, which is consistent with the definition of energy in the continuous case, yields a finite maximum allowable growth of the norms of the grid functions. Thus, such conditions will be identified here as *stability* conditions, see also [23, 31].

More specifically, in the following, each discrete Hamiltonian will be bounded from below by a positive-definite quadratic form. The inequality is expressed as

$$\mathfrak{h}^{n-1/2} = \mathfrak{h}^{1/2} \geq {}^{\mathsf{T}}(\mathbf{u}^{n-1/2})\mathbf{G}\ \mathbf{u}^{n-1/2} \tag{23}$$

where $\mathfrak{h}^{n-1/2}$ is the Hamiltonian at the given timestep, corresponding to a discrete version of the continuous Hamiltonian (10), $\mathbf{u}^{n-1/2}$ is a vector corresponding to the state, and $\mathbf{G}$ is a positive-definite quadratic form. In the following,

$$\mathbf{u}^{n-1/2} = \frac{\delta_{t-}}{\sqrt{2}}\ {}^{\mathsf{T}}[w_1^n, \ldots, w_{M-1}^n, \phi_{\frac{1}{2}}^n, \ldots, \phi_{M-\frac{1}{2}}^n] \tag{24}$$

The first equality in (23) expresses conservation of energy over time. Because $\mathbf{G}$ is positive-definite, one may write

$$\lambda_{\mathbf{G}}^{(min)}\|\mathbf{u}^{n-1/2}\|^2 \leq {}^{\mathsf{T}}(\mathbf{u}^{n-1/2})\mathbf{G}\ \mathbf{u}^{n-1/2} \tag{25}$$

where $\lambda_{\mathbf{G}}^{(min)} > 0$ is the minimum eigenvalue of the matrix $\mathbf{G}$. Hence, owing to (23) and (25), a bound on the growth of the norm of the state is found as

$$\|\mathbf{u}^{n-1/2}\| \leq \sqrt{\frac{\mathfrak{h}^{1/2}}{\lambda_{\mathbf{G}}^{(min)}}} \tag{26}$$

The derivation of the discrete Hamiltonians is rather lengthy, and in the following subsections, the results will be simply stated. The definitions of the matrices appearing below are given in Appendix A, whilst a complete proof of the non-negativity of the discrete Hamiltonians can be found in Appendix B.

3.5.1. Stability Condition For The Second-Order Accurate Scheme

For scheme (15), non-negativity of the associated discrete Hamiltonian is assured if and only if

$$k^2 < 4 \tag{27a}$$

$$h^2 \geq \frac{-B + \sqrt{\Delta}}{2A} \tag{27b}$$

where

$$A = (4 - k^2),\ B = k^4(\alpha - 1) - 4k^2(\alpha + \beta),\ C = 4\alpha\beta k^4,\ \Delta = B^2 - 4AC$$

Condition (27a) can be best understood by recalling the existence of the cutoff frequency $\omega_c = 1$, as per (6). In practice, there will be oscillating modes of frequency equal or larger then ω_c as the wavenumber tends to zero: the upper bound (27a) reflects this property.

3.5.2. Stability Condition For The Fourth-Order Accurate Scheme

Given the matrix

$$\mathbf{A}_{(4)} = \mathbf{1}^w + \left[\frac{(1-\theta_1)h^2}{2} + \frac{k^2}{4}(\alpha - 2(1-\theta_3))\right]\mathbf{D}^w_{xx} + \frac{(\alpha-1)(1-\theta_2)h^2k^2}{8}\mathbf{D}^w_{xxxx} \tag{28}$$

the non-negativity of the Hamiltonian associated with scheme (17) can be assured if and only if

$$\mathbf{A}_{(4)} > 0 \tag{29a}$$

$$\beta - \frac{(1-\theta_5)h^2}{2} \geq 0 \tag{29b}$$

$$1 + \frac{(1-\theta_4)h^2}{2} + \frac{k^2}{4}(1 - 2\theta_3) - \frac{k^2}{h^2}\left(\beta - \frac{(1-\theta_5)h^2}{2}\right) - \frac{4}{h^2\lambda^{(min)}_{\mathbf{A}_{(4)}}}\left(\frac{k^2}{4} - \frac{(1-\theta_3)k^2}{2}\right)^2 \geq 0 \tag{29c}$$

where $\lambda^{(min)}_{\mathbf{A}_{(4)}}$ is the minimum eigenvalue of the matrix $\mathbf{A}_{(4)}$, provided that it is positive definite from condition (29a).

3.5.3. Stability Condition For The Wideband Accurate Scheme

For scheme (21), a condition on the non-negativity of the associated Hamiltonian is

$$h^2 \geq \frac{(\alpha-1)k^2}{2\theta - 1}, \qquad \theta > \frac{1}{2} \tag{30}$$

Notice that the condition on θ is certainly satisfied by (22) and, under this particular choice, the number of grid intervals is equal to half the number of modes N below $1/2k$.

3.6. Numerical dispersion relation

The continuous dispersion relations derived in Section 2.2 have a numerical counterpart which is obtained through a transformation of the difference operators in the frequency domain [31].

In particular, the second time and space operators transform as

$$\delta_{tt} \to -\frac{4}{k^2}\underbrace{\sin^2(\omega k/2)}_{s_\omega}, \quad \delta_{xx} \to -\frac{4}{h^2}\underbrace{\sin^2(\gamma h/2)}_{s_\gamma}, \tag{31}$$

In the frequency domain, an equation for s_ω is obtained as

$$As_\omega^2 + Bs_\omega + C = 0, \tag{32}$$

where the coefficients A, B, C depend on h, k, θ_i as well as s_γ. For schemes (15), (17) and (21), they have rather lengthy expressions and are not reported here. Hence

$$s_\omega^\pm = \frac{-B \pm \sqrt{B^2 - 4AC}}{2A}$$

Numerical dispersion relations are obtained as

$$\omega_\pm = \frac{2}{k} \arcsin(\sqrt{s_\omega^\pm}) \tag{33}$$

If the wavenumber γ is restricted to take on values such that $0 \leq \gamma \leq \pi/h$, and h is chosen so as to satisfy the stability conditions, then $s_\omega^\pm$ is guaranteed to lie in the range $0 \leq s_\omega^\pm \leq 1$. It is useful to obtain the values of the dispersion relations in the limit of small wavenumbers, i.e. for $\gamma \to 0$. These are:

$$\lim_{\gamma \to 0} \omega_- = 0, \tag{34a}$$

$$\lim_{\gamma \to 0} \omega_+ = \frac{2}{k} \arcsin \sqrt{\frac{k^2}{k^2 + 4}}. \tag{34b}$$

Notice in particular that, in the limit of small k, $\omega_+ \to \omega_c$, which is consistent with (6). A plot of the numerical dispersion relations is shown in Figure 3.

3.6.1. Proof Of Fourth-Order Accuracy Of Scheme (17)

Scheme (17), under choice (19), leads to fourth-order accuracy in the numerical dispersion relation, in the limit of h, k going to zero. In order to prove this, one must first reduce the order of (29c), assuming that both h, k are small: hence, all quantities of order higher than four are removed, and the resulting inequality reads

$$Ah^4 + Bh^2 + C \geq 0 \tag{35}$$

with

$$A = 48\alpha^3\beta + 192\alpha^2\beta^2 + 24\alpha\beta^2 + 24\alpha\beta \tag{36a}$$

$$B = (-288\alpha^3\beta^2 - 48\alpha^3\beta - 192\alpha^2\beta^3 + 48\alpha^2\beta^2 - 48\alpha\beta^3 - 48\alpha\beta^2)k^2 \tag{36b}$$

$$C = 24\alpha\beta^2 k^4 (10\alpha^2\beta + 2\alpha^2 - 2\alpha\beta + \beta^2 + \beta) \tag{36c}$$

Inequality (35) is solved analytically by

$$h^2 \geq \beta k^2, \quad \text{if } \beta \geq \alpha \tag{37}$$

and it is possibile to verify that conditions (29a) and (29b) are indeed satisfied when h is chosen as close to the stability limit as possible, and when k is small enough. The condition $\beta \geq \alpha$ is also satisfied in general, for values of the tension of practical use.

The Taylor series of the difference operators in (17) is

$$\delta_{x\pm} = \partial_x + \frac{h^2}{24}\partial_x^3 \tag{38a}$$

$$\delta_{xx} = \partial_x^2 + \frac{h^2}{12}\partial_x^4 \tag{38b}$$

$$\delta_{xx}\delta_{xx} = \partial_x^4 + \frac{h^2}{6}\partial_x^6 \tag{38c}$$

$$\delta_{tt} = \partial_t^2 + \frac{k^2}{12}\partial_t^4 \tag{38d}$$

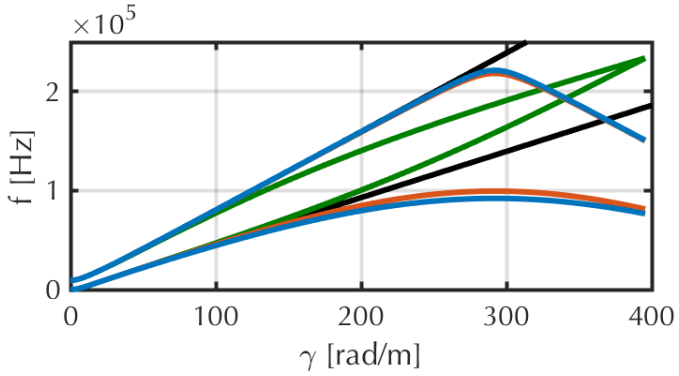

Figure 3: Dispersion relations of the numerical schemes. Solid black lines are the continuous model, blue lines are the second-order accurate scheme, red lines are the fourth-order accurate scheme, and green lines are the wideband accurate scheme. The picture is obtained for the thick beam, using a timestep $k = 1/8\omega_c$

where (38a) is valid when $\delta_{x\pm}$ are acting on an interleaved grid.

The Taylor-expanded discrete operators are now substituted in (17), and it is assumed that h, k approach zero while satisfying $h^2 \approx \beta k^2$. Under these assumptions, one may verify that the dispersion relation of (17) is such that

$$0 = \left(1 + \frac{\gamma^2 - 2\omega^2}{12\beta} h^2\right) \left(\omega^4 - \omega^2 - \gamma^2 + \alpha\gamma^2 - \alpha\gamma^2\omega^2 - \beta\gamma^2\omega^2 + \alpha\beta\gamma^4\right) + O(h^4) \tag{39}$$

and hence, recalling (4), the discrete dispersion relation approximates the continuous dispersion relation to fourth-order in h.

3.7. Matrix-Vector Form And Modes

It is useful to think of the space operators as matrices acting on column vectors $\mathbf{w}^n = [w_1^n, \ldots, w_{M-1}^n]^T$ and $\boldsymbol{\phi}^n = [\phi^n_{\frac{1}{2}}, \ldots, \phi^n_{M-\frac{1}{2}}]^T$. Schemes (15), (17), (21) can be written as

$$\mathbf{M} \begin{pmatrix} \delta_{tt}\mathbf{w}^n \\ \delta_{tt}\boldsymbol{\phi}^n \end{pmatrix} = -\mathbf{K} \begin{pmatrix} \mathbf{w}^n \\ \boldsymbol{\phi}^n \end{pmatrix} \tag{40}$$

The matrices for the second-order, fourth-order and wideband accurate schemes are given as

$$\mathbf{M}_{(2)} = \begin{pmatrix} \mathbf{1}^w & \mathbf{0}^\phi \\ \mathbf{0}^w & \mathbf{1}^\phi \end{pmatrix}$$

$$\mathbf{K}_{(2)} = \begin{pmatrix} -\alpha\mathbf{D}^w_{xx} & \mathbf{D}^\phi_{x-} \\ -\mathbf{D}^w_{x+} & \mathbf{1}^\phi - \beta\mathbf{D}^\phi_{xx} \end{pmatrix}.$$

$$\mathbf{M}_{(4)} = \begin{pmatrix} \mathbf{1}^w + \left(\frac{(1-\theta_1)h^2}{2} - \frac{(1-\theta_3)k^2}{2}\right)\mathbf{D}^w_{xx} & \frac{(1-\theta_3)k^2}{2}\mathbf{D}^\phi_{x-} \\ -\frac{(1-\theta_3)k^2}{2}\mathbf{D}^w_{x+} & \left(1 + \frac{(1-\theta_4)h^2}{2} + \frac{(1-\theta_3)k^2}{2}\right)\mathbf{1}^\phi \end{pmatrix}$$

$$\mathbf{K}_{(4)} = \begin{pmatrix} -\alpha\mathbf{D}^w_{xx} + (1-\alpha)\frac{(1-\theta_2)h^2}{2}\mathbf{D}^w_{xxxx} & \mathbf{D}^\phi_{x-} \\ -\mathbf{D}^w_{x+} & \mathbf{1}^\phi - \left(\beta - \frac{(1-\theta_5)h^2}{2}\right)\mathbf{D}^\phi_{xx} \end{pmatrix}.$$

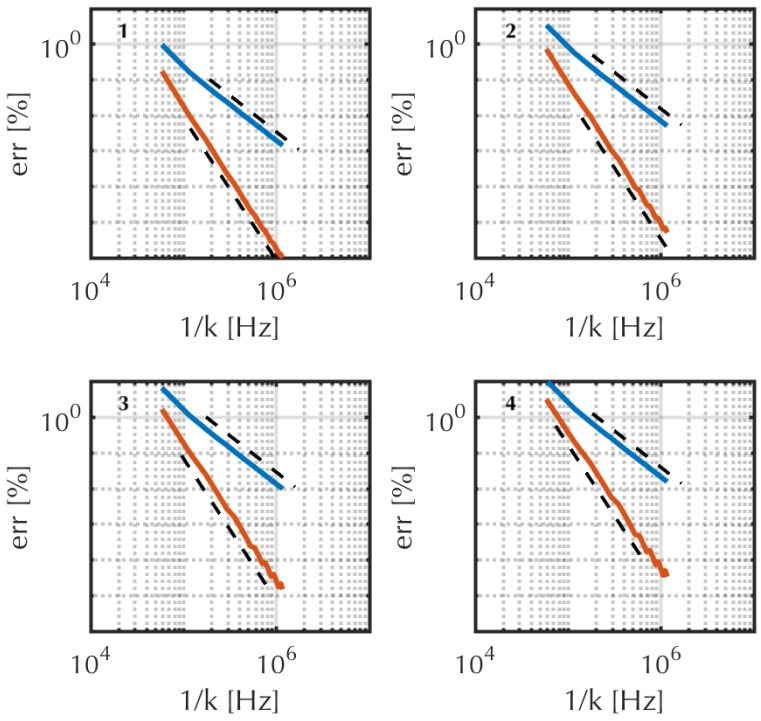

Figure 4: Convergence of the first four eigenfrequencies of the thick beam, for scheme (15) (blue) and (17) (red). Black dashed lines of slope 2 and 4 are also drawn, for reference.

$$\mathbf{M}_{(W)} = \begin{pmatrix} \mathbf{1}^w + \left(\frac{(1-\theta)h^2}{2} - \frac{k^2}{4}\right)\mathbf{D}^w_{xx} & \frac{k^2}{4}\mathbf{D}^\phi_{x-} \\ -\frac{k^2}{4}\mathbf{D}^w_{x+} & \left(1+\frac{k^2}{4}\right)\mathbf{1}^\phi + \frac{(1-\theta)h^2}{2}\mathbf{D}^\phi_{xx} \end{pmatrix}$$

$$\mathbf{K}_{(W)} = \begin{pmatrix} -\alpha\mathbf{D}^w_{xx} & \mathbf{D}^\phi_{x-} \\ -\mathbf{D}^w_{x+} & \mathbf{1}^\phi - \beta\mathbf{D}^\phi_{xx} \end{pmatrix}.$$

In order to obtain the numerical modal frequencies, (40) is transformed into an eigenvalue problem. Recalling the z-transform of δ_{tt} as per (31), one may obtain the numerical eigenfrequencies as

$$\omega = \frac{2}{k}\arcsin\frac{k\sqrt{\mathrm{eig}(\mathbf{M}^{-1}\mathbf{K})}}{2} \tag{41}$$

Figure 4 shows the convergence of the first four eigenfrequencies, for the second-order accurate and fourth-order accurate schemes, highlighting the expected convergence trend.

Figure 5(a) shows the modal distributions of the three schemes, and Figure 5(b) is the percentage error. The second and fourth-order accurate schemes, despite providing convergence with a known trend, are poorly behaved at higher frequencies: the minimum grid size for both schemes is too large to account for all the modes falling within the Nyquist range, and the modal distribution gets highly distorted above the cutoff frequency. The wideband accurate scheme, on the other hand, makes use of the free parameters to accomodate for all the modes, shrinking the grid spacing.

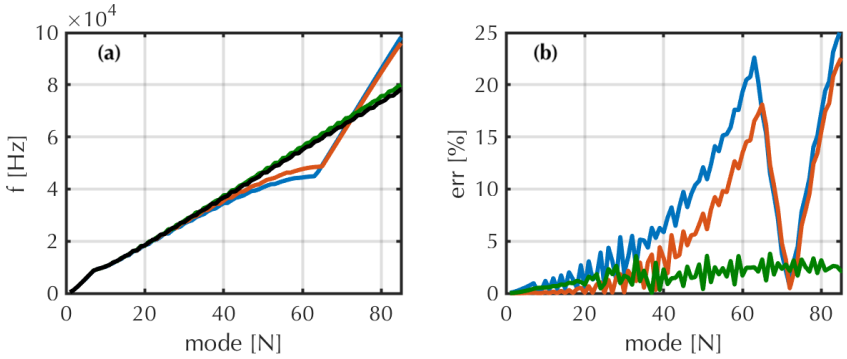

Figure 5: Numerical modes of the Timoshenko scheme. For the two figures, solid black is the continuous model, blue is the second-order accurate scheme, red is the fourth-order accurate scheme, and green line is the wideband accurate scheme. The figures are obtained for the thick beam, using a timestep $k = 1/8\omega_c$(a): modal frequencies. (b): percentage error of the modal frequencies

Indeed, the wideband accurate scheme may be employed anytime a high resolution is required at all scales, and especially at smaller wavelengths: for example, in resolving transients.

3.8. The Euler-Bernoulli And Shear Models

Now that the schemes for the Timoshenko system have been optimised and validated, the finite difference schemes used for the shear and Euler-Bernoulli models are now given. The treatment here will be rather quick, as the mechanics of the proofs for order accuracy and stability mimic those already given for the Timoshenko schemes. Thus, many of the following results are stated without a proof, but these schemes are conservative, and the non-negativity of the associated Hamiltonians are sufficient and necessary conditons for numerical stability.

3.8.1. Second-Order Accurate Scheme For The Shear Beam

A second-order accurate scheme for the shear model can be obtained by direct substitution of the discrete difference operators of Table 2 into (13). This gives

$$(1 - \beta\delta_{xx})\delta_{tt}w_m^n = (\alpha - 1)\delta_{xx}w_m^n - \alpha\beta\delta_{xx}\delta_{xx}w_m^n \tag{42}$$

Simply-supported end condititions are derived as

$$w_0^n = \delta_{xx}w_0^n = w_M^n = \delta_{xx}w_M^n = 0 \tag{43}$$

von Neumann analysis yields the following stability condition

$$h^2 \geq \frac{-B + \sqrt{B^2 - 4C}}{2}, \tag{44}$$

where

$$B = 4\beta - (\alpha - 1)k^2, \qquad C = -4\alpha\beta k^2.$$

3.8.2. Fourth-Order Accurate Scheme For The Shear Beam

A parameterized scheme for the shear model is given here as

$$(1 - \beta q(\theta_1)\delta_{xx})\delta_{tt}w_m^n = (\alpha - 1)s(\theta_2)\delta_{xx}w_m^n - \alpha\beta\delta_{xx}\delta_{xx}w_m^n \tag{45}$$

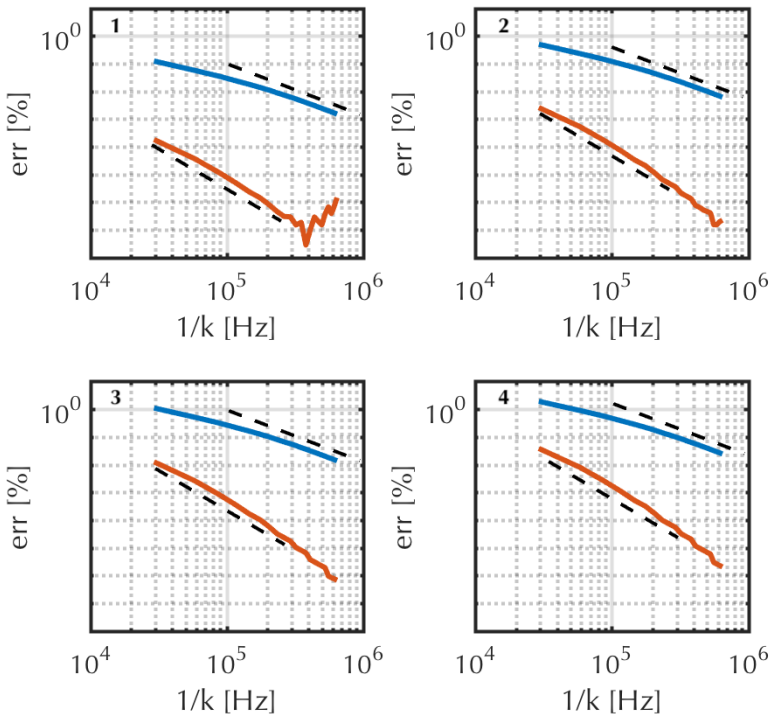

Figure 6: Convergence of the first four eigenfrequencies of the medium beam, for scheme (42) (blue) and (45) (red). Black dashed lines of slope 2 and 4 are also drawn, for reference.

where $s(\theta)$, $q(\theta)$ are as per (18). Simply-supported end conditions are of the form (43).

For fourth-order accuracy, the free parameters must be chosen as

$$\theta_1 = \frac{\alpha + 6\alpha\beta + 1}{6\alpha\beta}, \quad \theta_2 = \frac{5}{6} \tag{46}$$

Von Neumann analysis on this scheme yields

$$h^2 \geq \frac{-B + \sqrt{B^2 - 4AC}}{2A} \tag{47}$$

where

$$A = (1 + 2\beta(1 - \theta_1)), \quad B = 4\beta - (\alpha - 1)k^2(2\theta_2 - 1), \quad C = -4\alpha\beta k^2$$

Fourth-order accuracy is given in terms of the dispersion relation, as for the Timoshenko system. In the limit of small h, k, the grid spacing in (47), chosen as close to the stability limit as possible, becomes

$$h^2 \approx \frac{\alpha k^2}{2\theta_2 - 1} \tag{48}$$

When the Taylor-expanded difference operators (38) are substituted into (45), one obtains the following numerical dispersion relation

$$0 = \left(1 - \frac{\omega^2 + 2\alpha\gamma^2}{12\alpha}h^2\right)\left(-\omega^2(\beta\gamma^2 + 1) + \gamma^2(\alpha - 1) + \alpha\beta\gamma^4\right) + O(h^4) \tag{49}$$

which is a fourth-order accurate approximation to the continuous dispersion relation [6]. Fig. 6 illustrates the convergence of the second-order and of the fourth-order accurate schemes, for the first four eigenfrequencies, highlighting the expected trend as the the time step becomes small. Fig. 7 depicts the modal distributions of the three schemes, as well as the associated error, for a reference time step $k = 2/\omega_c$.

3.8.3. Wideband Accurate Scheme For The Shear Beam

A wideband accurate finite difference scheme for the shear model (13) is given as

$$(1 - \beta\delta_{xx})s(\theta)\delta_{tt}w_m^n = (\alpha - 1)\delta_{xx}w_m^n - \alpha\beta\delta_{xx}\delta_{xx}w_m^n \tag{50}$$

with $s(\theta)$ given in (18). The value for θ is given as

$$\theta = \frac{1}{2} + \frac{(\alpha - 1)k^2\bar{h}^2 + 4\alpha\beta k^2}{2\bar{h}^2(\bar{h}^2 + 4\beta)}, \tag{51}$$

where

$$\bar{h} = \frac{L_0}{M}.$$

This value for θ is analogous to the one used for the wideband Timoshenko scheme, (22): the number of grid spacings matches the number of modes M falling within the Nyquist limit $1/2k$. The stability conditions for this scheme can be given as

$$h^2 \geq \frac{-B + \sqrt{B^2 - 4(2\theta - 1)C}}{2(2\theta - 1)}, \tag{52}$$

where

$$B = 4\beta(2\theta - 1) - (\alpha - 1)k^2, \qquad C = -4\alpha\beta k^2.$$

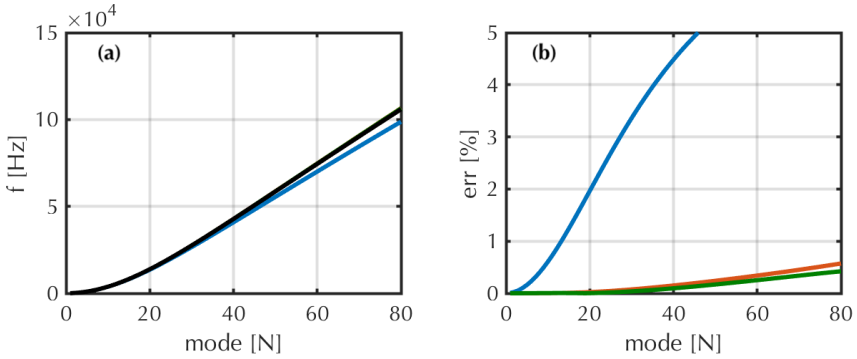

Figure 7: Numerical modes of the shear scheme. For the two figures, solid black is the continuous model, blue is the second-order accurate scheme, red is the fourth-order accurate scheme, and green line is the wideband accurate scheme. The figures are obtained for the medium beam, using a timestep $k = 2/\omega_c$(a): modal frequencies. (b): percentage error of the modal frequencies

3.8.4. Second-Order Accurate Scheme For The Euler-Bernoulli Beam

A second-order accurate scheme for the Euler-Bernoulli beam is obtained by direct substitution of the difference operators of Table (2) into (14). This gives

$$\delta_{tt} w_m^n = (\alpha - 1)\delta_{xx} w_m^n - \beta \delta_{xx}\delta_{xx} w_m^n \tag{53}$$

with simply-supported end conditions of the form (43). von Neumann analysis yields the following stability condition

$$h^2 \geq \frac{k^2(\alpha - 1) + \sqrt{k^4(\alpha - 1)^2 + 16\beta k^2}}{2} \tag{54}$$

3.8.5. Fourth-Order Accurate Scheme For The Euler-Bernoulli Beam

Fourth-order accuracy may be achieved by employing two free parameters, in the following way

$$s(\theta_1)\delta_{tt} w_m^n = \alpha s(\theta_2)\delta_{xx} w_m^n - \beta \delta_{xx}\delta_{xx} w_m^n, \quad \theta_1 = \frac{2}{3}, \quad \theta_2 = \frac{5}{6} \tag{55}$$

where $s(\theta)$ is defined in (18). The stability condition, derived from von Neumann analysis, yields

$$h^2 \geq \frac{k^2(\alpha - 1)(2\theta_2 - 1) + \sqrt{k^4(\alpha - 1)^2(2\theta_2 - 1)^2 + 16\beta k^2(2\theta_1 - 1)}}{2(2\theta_1 - 1)} \tag{56}$$

In the limit as h, k become small, the stability limit is approximately

$$h^2 \approx \frac{2\beta^{1/2} k}{(2\theta_1 - 1)^{1/2}} \tag{57}$$

Calculating the numerical dispersion relation of (55), and Taylor-expanding the difference operators according to (38), one gets

$$0 = \left(1 - \frac{\gamma^2 h^2}{6}\right)\left(\beta\gamma^2 + (\alpha - 1)\gamma^2 - \omega^2\right) + O(h^4) \tag{58}$$

which is a fourth-order accurate approximation to the continuous dispersion relation [6]. Fig. 8 shows the convergence of the eigenfrequencies for the second-order and the fourth-order accurate

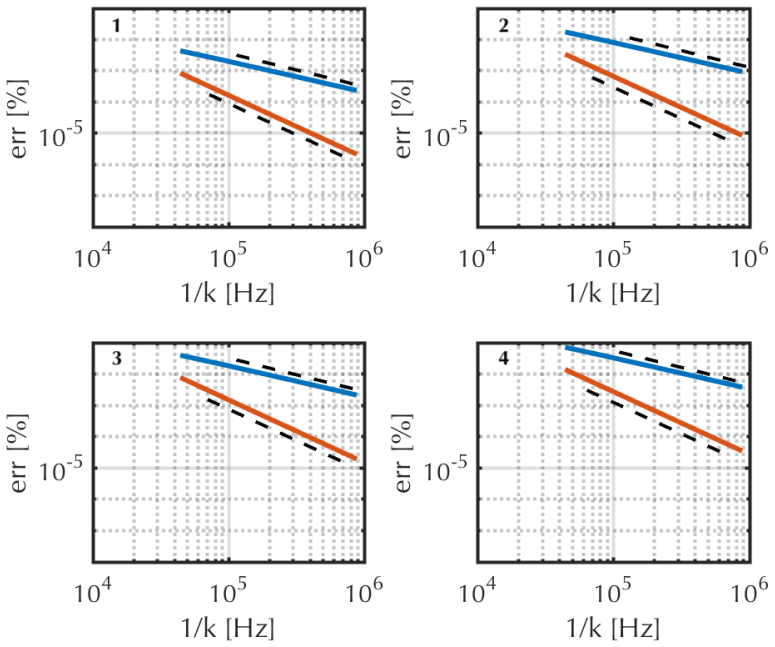

Figure 8: Convergence of the first four eigenfrequencies of the thin beam, for scheme (53) (blue) and (55) (red). Black dashed lines of slope 1 and 2 are also drawn, for reference.

schemes. Notice that, the slopes are only half of those obtained for the shear and for the Timoshenko schemes. However, slopes of two and four are recovered in the grid spacing, as per (57). Fig. 9 depicts the distribution of the modal frequencies, and related errors, for the three schemes, using a reference time step $k = 1/44100$.

3.8.6. Wideband Accurate Scheme For The Euler-Bernoulli Beam

A wideband accurate scheme for the Euler-Bernoulli beam can be given as

$$s(\theta)\delta_{tt}w_m^n = (\alpha - 1)\delta_{xx}w_m^n - \beta\delta_{xx}\delta_{xx}w_m^n \tag{59}$$

with $s(\theta)$ given in (18). The value for θ is given as

$$\theta = \frac{1}{2} + \frac{(\alpha - 1)k^2\bar{h}^2 + 4\beta k^2}{2\bar{h}^4}. \tag{60}$$

where

$$\bar{h} = \frac{L_0}{M}.$$

This value for θ guarantees that the number of grid spacings matches the number of modes M falling within the Nyquist limit, $1/2k$.

The stability conditions for this scheme, derived from von Neumann analysis, is

$$h^2 \geq \frac{-B + \sqrt{B^2 - 4(2\theta - 1)C}}{2(2\theta - 1)}, \tag{61}$$

where

$$B = -(\alpha - 1)k^2, \qquad C = -4\beta k^2.$$

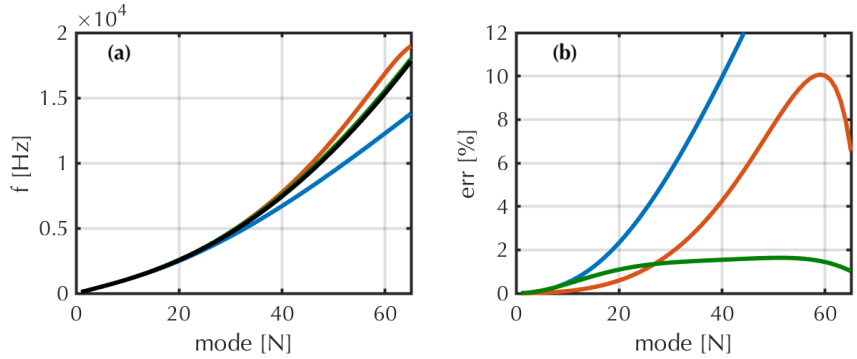

Figure 9: Numerical modes of the Euler-Bernoulli schemes. For the two figures, solid black is the continuous model, blue is the second-order accurate scheme, red is the fourth-order accurate scheme, and green line is the wideband accurate scheme. The figures are obtained for the medium beam, using a timestep $k = 1/44100$(a): modal frequencies. (b): percentage error of the modal frequencies

4. Numerical Results

In this section, the simulations of the three case studies (thick beam, medium beam, thin beam) are analysed. It is useful to introduce a dimensionless parameter s, called the *slenderness ratio* and defined as

$$s = L_0\sqrt{\frac{A}{I}}. \tag{62}$$

This parameter is useful when comparing the three models. As this parameter gets large, the cutoff frequency ω_c tends to infinity, meaning that the motion is almost entirely flexural. For the three beams under consideration, s is

$$s = 2000 \text{ for the thin beam}, \quad s = 200 \text{ for the medium beam}, \quad s = 20 \text{ for the thick beam}.$$

This parameter indicates which model to use, given the beam radius [4]. For small values ($s < 100$) the Timoshenko model should be used, and for large values ($s > 1000$) Euler-Bernoulli can be safely employed. For intermediate values, the shear model can be used.

The second-order, fourth-order and wideband schemes are compared in each case. The initial conditions for the simulations are in the form of a centered raised cosine function, with zero velocity. Thus, at the time $t = 0$ the displacement w is of the form

$$w(x,0) = \begin{cases} 0.5\left(\left(1+\cos(\pi\frac{x-0.5L_0}{0.3}\right)\right) & \text{if } |x-0.5L_0| \leq 0.3 \\ 0 & \text{if } |x-0.5L_0| > 0.3 \end{cases}$$

whilst for the shear angle the initial conditions are such that $\phi(x,0) = 0$. Output is extracted at m_O, i.e. the nearest grid point to the left of $x_O = 0.23L_0$.

4.1. Thick Beam

Fig. 10 shows a few snapshots of the thick beam at the initial and later instants. A scheme with time step refinement factor of 10 yields effectively converged solutions for the second-order, fourth-order, and wideband schemes, used here for benchmarking. When the schemes are run with a larger timestep, divergence from the benchmark is apparent, as expected. Fig. 11(a) shows a plot of the waveform at the output for the oversampled schemes: the three schemes yield a converged solution. Fig. 11(b) shows the solutions produced by the schemes using a larger timestep. Fig.

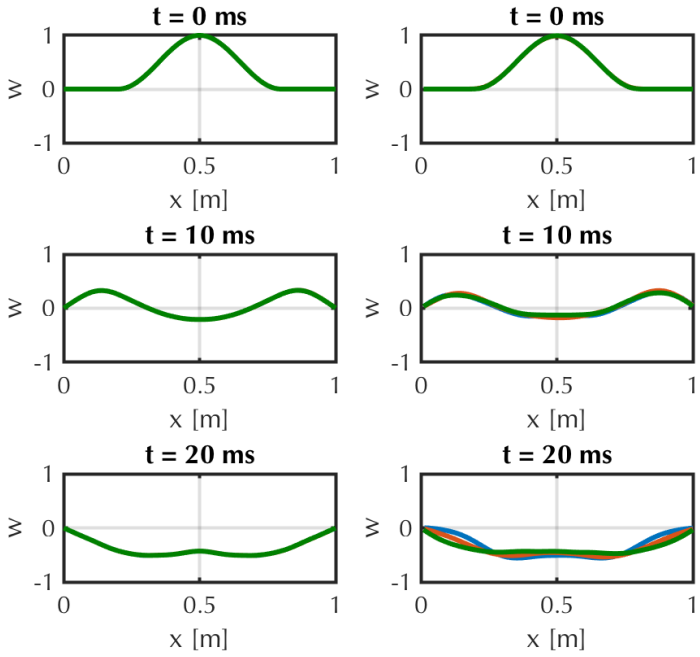

Figure 10: Snapshots of the thick beam simulated via the Timoshenko schemes. Blue: second-order, red: fourth-order, green: wideband. The snapshots on the left and on the right are obtained using, respectively, a timestep $k = 1/64\omega_c$, and a timestep $k = 1/6.4\omega_c$

11(c) is a representation of the time domain error of the schemes of Fig. 11(b), compared against the converged solution. The error is caculated on a per-sample basis, using a downsampled version of the converged solution. A low-pass filter is applied to the waveforms so obtained, to display the envelope of the error over time. In Fig. 11(c), the error of the wideband scheme is the smallest up to about 4 ms, before being overtaken by the fourth-order accurate scheme. The interpretation of this result is best understood by considering the higher resolving power of the wideband scheme for short wavelengths: in the initial instants, shorter wavelengths dominate the dynamics. After a few cycles, the overall envelope of the vibration will be dictated by longer wavelengths, which are best resolved by the fourth-order accurate scheme.

4.2. Medium Beam

Snapshots of the medium beam, simulated via the shear schemes, are depicted in Fig. 12. The snapshots compare the simulations obtained using oversampled schemes, with an oversampling factor of 20, and the simulations obtained using reference value for the timestep, $k = 1/0.3\omega_c$. As for the thick beam, the oversampled schemes yield a converged solution, visible both in the snapshots of Fig. 12, and in Fig. 13(a). Fig. 13(c) is again a representation of the envelope of the time domain error of the schemes run using the reference time step, versus the converged solution. In this case, the error of the wideband scheme remains below the error of the fourth-order schemes, for the times indicated.

4.3. Thin Beam

The snapshots for the thin beam are plotted in Fig. 14. The reference timestep is in this case $k = 1/44100s$, and the oversampled schemes are run with a timestep $k = 1/882000s$ (thus

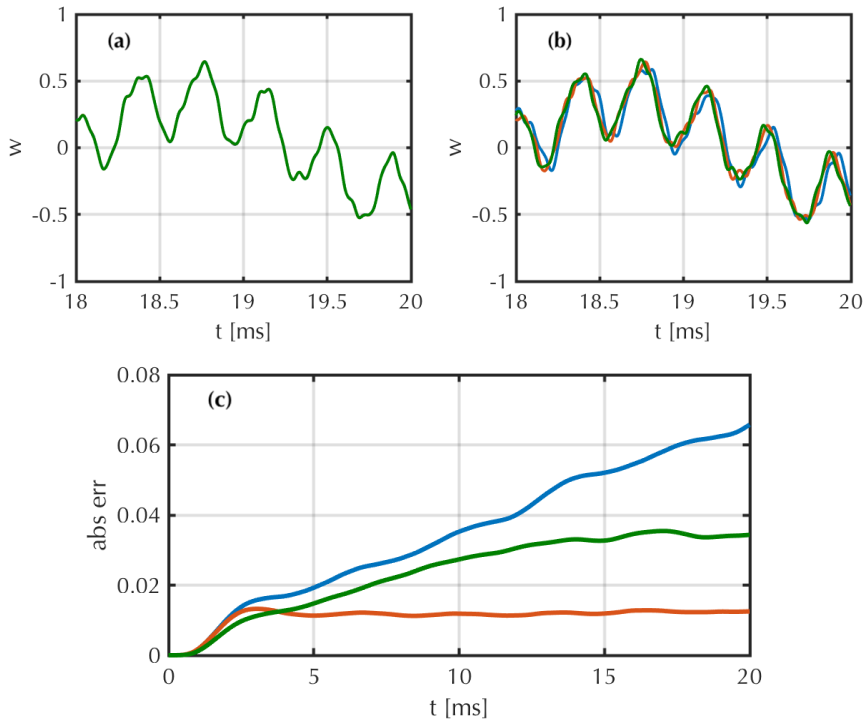

Figure 11: Time domain waveforms of the thick beam, obtained using the Timoshenko schemes. Blue: second-order, red: fourth-order, green: wideband. (a): oversampled simulations, using $k = 1/64\omega_c$. (b): $k = 1/6.4\omega_c$. (c): absolute error $|w - \tilde{w}|$, where $\tilde{w}$ is the downsampled congerged solution drawn in panel (a)

wiht an oversampling factor of 20). As for the Timoshenko and for the shear schemes, during the initial instants the wideband scheme overperforms the fourth-order accurate scheme, because of the increased resolving power at small scales. As time passes, larger wavelengths dictate the overall envelope of the motion, and the fourth-order accurate scheme overtakes the wideband scheme.

5. Conclusions

In this work, finite difference time domain schemes with various degrees of accuracy have been proposed for the simulation of the most widely used engineering beam models: Timoshenko, shear, and Euler-Bernoulli. For each of the three models, three schemes have been proposed, with second-order, fourth-order, and wideband accuracy. The schemes have been constructed by means of second-order accurate finite difference operators, as well as a number of free parameters, tuned so to achieve the desired accuracy. The order of accuracy is understood to be in terms of the dispersion relation, i.e. the numerical dispersion relations approximate the continuous ones at the given degree. Moreover, in order to obtained the desired order of accuracy, appropriate relations between the timestep k and the grid spacing h must be fulfilled in the limit as k, h become small. Such relations have been derived from stability analysis, and in particular via Hamiltonian methods (detailed in Appendix B). Settings for the free parameters have been given for the fourth-order accurate schemes. The accuracy of the scheme is valid in the time domain over infinite grids, as the boundary conditions remain second-order accurate. The fourth-order scheme presented here has an implicit character, and it requires the inversion of a matrix at each time-step. Another type of scheme, here called wideband, has been presented: this scheme is best suited to reduce the error at all wavelengths, despite a low formal order of accuracy. The wideband schemes are

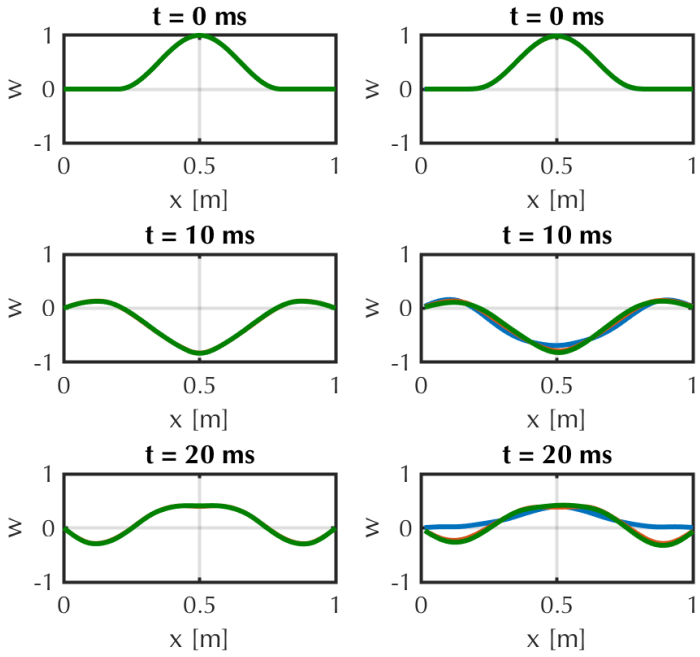

Figure 12: Snapshots of the medium beam simulated via the shear schemes. Blue: second-order, red: fourth-order, green: wideband. The snapshots on the left and on the right are obtained using, respectively, a timestep $k = 1/6\omega_c$, and a timestep $k = 1/0.3\omega_c$

able to calculate the eigenfrequencies of a given beam within small error bounds (about 2%) across the whole spectrum, using reference time steps. In the time domain, they are best suited to represent transients, i.e. portions of the waveform where small wavelengths dominate the dynamics. Over longer periods, the fourth-order accurate schemes give the smallest error with respect to the converged solution, on a per-sample basis. Analytic results have been given in order to tune the θ-parameters for the wideband schemes: essentially, the free parameters adjust the number of grid points so to match the number of analytic modes within the Nyquist limit. This has a prominent beneficial effect for the Timoshenko model: the second-order and the fourth-order schemes fail dramatically at representing small wavelengths. The wideband schemes employed in this work have a simpler form than the fourth-order accurate schemes, and stability conditions can be deduced with much less analytical work. However, refined schemes making use of more free parameters could be designed, so to improve accuracy at larger scales. This particular aspect has not been investigated here, but is left as future work. In this way, finite difference wideband schemes could be desinged, so to give spectral-like spatial resolution, yet retaining the two-step temporal form. Inclusion of losses, as well as source terms, may be realised in a straightforward manner from the templates given here.

6. Acknowledgement

The first author would like to thank the Leverhulme Trust, who funded this work with an Early Career Fellowship.

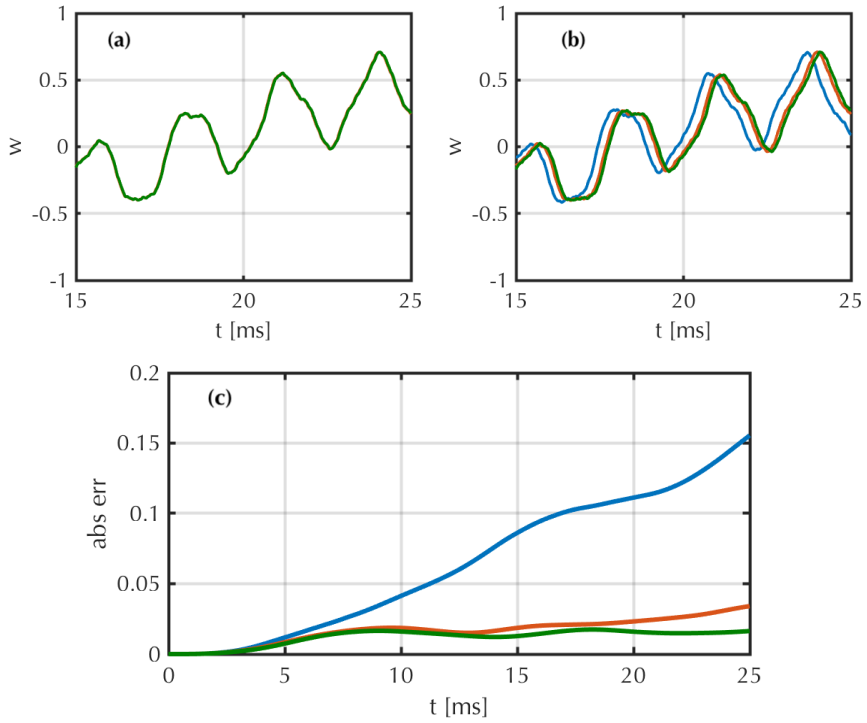

Figure 13: Time domain waveforms of the medium beam, obtained using the shear schemes. Blue: second-order, red: fourth-order, green: wideband. (a): oversampled simulations, using $k = 1/6\omega_c$. (b): $k = 1/0.3\omega_c$. (c): absolute error $|w - \tilde{w}|$, where $\tilde{w}$ is the downsampled congerged solution drawn in panel (a)

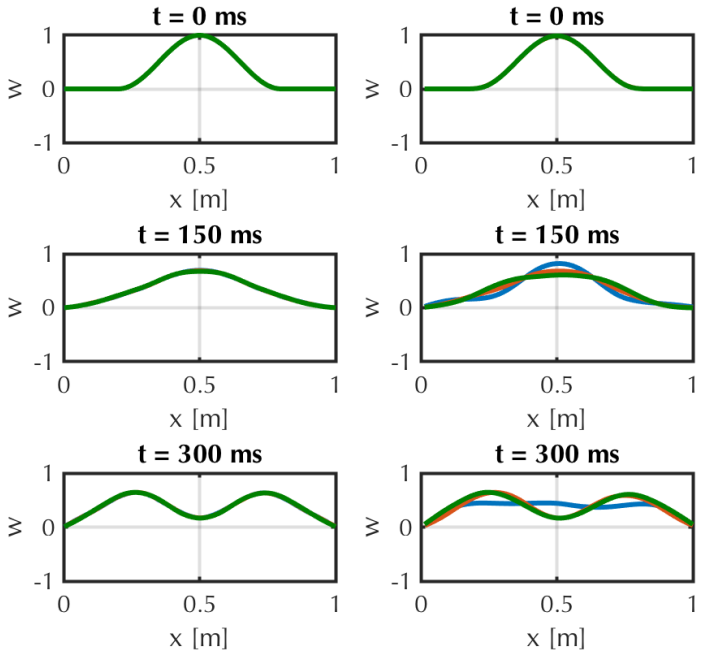

Figure 14: Snapshots of the thin beam simulated via the Euler-Bernoulli schemes. Blue: second-order, red: fourth-order, green: wideband. The snapshots on the left and on the right are obtained using, respectively, a timestep $k = 1/882000s$, and a timestep $k = 1/44100s$

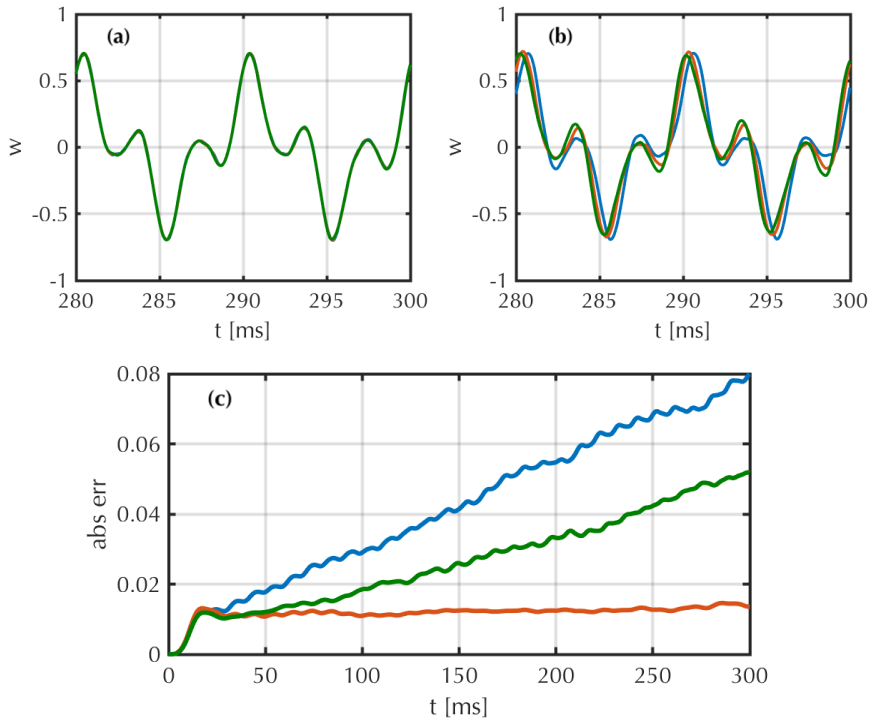

Figure 15: Time domain waveforms of the thin beam, obtained using the Euler-Bernoulli schemes. Blue: second-order, red: fourth-order, green: wideband. (a): oversampled simulations, using $k = 1/882000$. (b): $k = 1/44100$. (c): absolute error $|w - \tilde{w}|$, where $\tilde{w}$ is the downsampled congerged solution drawn in panel (a)

7. References

[1] K. F. Graff. *Wave Motion in Elastic Solids*. Dover Publications, New York, USA, 1991.

[2] S. S Rao and Y. F. Fah. *Mechanical Vibrations; 5th ed. in SI units*. Prentice Hall, Singapore, 2011.

[3] G. Jelenić and M. A. Crisfield. Geometrically exact 3D beam theory: implementation of a strain-invariant finite element for statics and dynamics. *Comp. Methods In Appl. Mech. Eng.*, 171:141–171, 1997.

[4] S.M. Han, H. Benaroya, and T. Wei. Dynamics of transversely vibrating beams using four engineering theories. *J. Sound Vib.*, 225(3):935–988, 1999.

[5] B.A.H. Abbas and J. Thomas. The second frequency spectrum of Timoshenko beams. *J. Sound Vib.*, 51(1):123–137, 1977.

[6] M. Ducceschi and S. Bilbao. Linear stiff string vibrations in musical acoustics: Assessment and comparison of models. *J. Acoust. Soc. Am.*, 140(4):2445–2454, 2016.

[7] A. Mirzabeigy, M. Haghpanahi, and R. Madoliat. A new finite element formulation for buckling and free vibration analysis of Timoshenko beams on variable elastic foundation. *J. Solid Mech.*, 9(2):276–290, 2017.

[8] R. Davis, R.D. Henshell, and G.B. Warburton. A Timoshenko beam element. *J. Sound Vib.*, 22(4):475–487, 1972.

[9] D.J. Dawe. A Finite Element for the vibration analysis of Timoshenko beams. *J. Sound Vib.*, 60(1):11–20, 1978.

[10] P. Subramanian. Dynamic analysis of laminated composite beams using higher order theories and Finite Elements. *Compos. Struct.*, 73(3):342–353, 2006.

[11] J. Thomas and B.A.H. Abbas. Finite Element model for dynamic analysis of Timoshenko beam. *J. Sound Vib.*, 41(3):291–299, 1975.

[12] P.R. Heyliger and J.N. Reddy. A higher order beam Finite Element for bending and vibration problems. *J. Sound Vib.*, 126(2):309–326, 1988.

[13] Z. Friedman and J.B. Kosmatka. An improved two-node Timoshenko beam Finite Element. *Comput. Struct.*, 47(3):473–481, 1993.

[14] R.S. Gupta and S.S. Rao. Finite Element eigenvalue analysis of tapered and twisted Timoshenko beams. *J. Sound Vib.*, 56(2):187–200, 1978.

[15] S.S. Rao and R.S. Gupta. Finite Element vibration analysis of rotating Timoshenko beams. *J. Sound Vib.*, 242(1):103–124, 2001.

[16] B. Semper. Semi-discrete and fully discrete Galerkin methods for the vibrating Timoshenko beam. *Comput. Methods In Appl. Mech. Eng.*, 117(3):353–360, 1994.

[17] N.F.J. van Rensburg and A.J. van der Merwe. Natural frequencies and modes of a Timoshenko beam. *Wave Motion*, 44(1):58 – 69, 2006.

[18] J. Lee and W.W. Schultz. Eigenvalue analysis of Timoshenko beams and axisymmetric Mindlin plates by the pseudospectral method. *J. Sound Vib.*, 269(3):609 – 621, 2004.

[19] A. Civalek and O. Kiracioglu. Free vibration analysis of Timoshenko beams by DSC method. *Int. J. Numer. Method Biomed. Eng.*, 26(12):1890–1898, 2010.

[20] A.S Sarigül and G. Aksu. A finite difference method for the free vibration analysis of stepped Timoshenko beams and shafts. *Mech. Mach. Theory*, 21(1):1 – 12, 1986.

[21] Fu le Li and Zhi zhong Sun. A finite difference scheme for solving the Timoshenko beam equations with boundary feedback. *J. Comput. Appl. Math.*, 200(2):606–627, 2007.

[22] D. S. Almeida Junior. Conservative Semidiscrete Difference Schemes for Timoshenko Systems. *J. Appl. Math.*, 2014:7 pages, 2014.

[23] J. Chabassier and S. Imperiale. Stability and dispersion analysis of improved time discretisation for prestressed Timoshenko systems. Application to the stiff piano string. *Wave Motion*, 50:456–480, 2013.

[24] J. Chabassier, A. Chaigne, and P. Joly. Modeling and simulation of a grand piano. *J. Acoust. Soc. Am.*, 134(1):648–665, 2013.

[25] R.F Warming and B.J Hyett. The modified equation approach to the stability and accuracy analysis of finite-difference methods. *J. Comput. Phys.*, 14(2):159 – 179, 1974.

[26] G. Cohen and P. Joly. Construction analysis of fourth-order finite difference schemes for the acoustic wave equation in nonhomogeneous media. *SIAM J. Numer. Anal.*, 33(4):1266 – 1302, 1996.

[27] P. Joly and J. Rodríguez. Optimized higher order time discretization of second order hyperbolic problems: Construction and numerical study. *J. Comput. Appl. Math.*, 234(6):1953 – 1961, 2010.

[28] M.A. Dablian. The application of high order differencing for the scalar wave equation. *Geophysics*, 51:54 – 56, 1986.

[29] S. Bilbao and B. Hamilton. Higher-order accurate two-step finite difference schemes for the many-dimensional wave equation. *J. Comput. Phys.*, 367:134 – 165, 2018.

[30] S. K. Lele. Compact finite difference schemes with spectral-like resolution. *J. Comp. Phys.*, 103(1):16 – 42, 1992.

[31] S. Bilbao. *Numerical Sound Synthesis: Finite Difference Schemes and Simulation in Musical Acoustics*. Wiley, Chichester, UK, 2009.

[32] B. Gustafsson, H-O. Kreiss, and J. Oliger. *Time-Dependent Problems and Difference Methods*. Wiley, Hoboken, 2013.

[33] M. Svärd and J. Nordström. Review of summation-by-parts schemes for initial-boundary-value problems. *J. Comp. Phys.*, 268:17 – 38, 2014.

Appendix A. Matrix Notation

In the text, extensive use of matrix notation is used. The explicit forms of the matrices are given here below. The grid spacing h is assumed to divide the domain length L_0 evenly, such that $L_0/h = N$ for some integer M. Under simply supported conditions, w_m^n is defined for $m = 1, \ldots, M-1$ and $\phi_{m+1/2}^n$ for $m = 0, \ldots, M-1$.

$$\mathbf{0}^w = \begin{pmatrix} 0 & 0 & & \\ 0 & 0 & \ddots & \\ & \ddots & \ddots & 0 \\ & & 0 & 0 \end{pmatrix}, \text{ is } M \times (M-1) \qquad \mathbf{0}^\phi = \begin{pmatrix} 0 & 0 & & \\ 0 & 0 & \ddots & \\ & \ddots & \ddots & 0 \\ & & 0 & 0 \end{pmatrix}, \text{ is } (M-1) \times M.$$

$$\mathbf{1}^w = \begin{pmatrix} 1 & 0 & & \\ 0 & 1 & \ddots & \\ & \ddots & \ddots & 0 \\ & & 0 & 1 \end{pmatrix}, \text{ is } (M-1) \times (M-1) \qquad \mathbf{1}^\phi = \begin{pmatrix} 1 & 0 & & \\ 0 & 1 & \ddots & \\ & \ddots & \ddots & 0 \\ & & 0 & 1 \end{pmatrix}, \text{ is } M \times M.$$

$$\mathbf{D}_{x+}^w = \frac{1}{h} \begin{pmatrix} 1 & 0 & 0 & 0 \\ -1 & 1 & 0 & 0 \\ 0 & -1 & 1 & 0 \\ & & \ddots & \ddots \\ & & & -1 \end{pmatrix}, \text{ is } M \times (M-1), \qquad \mathbf{D}_{x-}^\phi = -^T\mathbf{D}_{x+}^w.$$

$$\mathbf{D}_{xx}^w = \frac{1}{h^2} \begin{pmatrix} -1 & 1 & 0 & & & \\ 1 & -2 & 1 & 0 & & \\ 0 & 1 & -2 & 1 & 0 & \\ & \ddots & \ddots & \ddots & \ddots & 0 \\ & & 0 & 1 & -2 & 1 \\ & & & 0 & 1 & -1 \end{pmatrix}, \text{ is } (M-1) \times (M-1), \qquad \mathbf{D}_{xxxx}^w = (\mathbf{D}_{xx}^w)^2.$$

$$\mathbf{D}_{xx}^\phi = \frac{1}{h^2} \begin{pmatrix} -2 & 1 & 0 & & & \\ 1 & -2 & 1 & 0 & & \\ 0 & 1 & -2 & 1 & 0 & \\ & \ddots & \ddots & \ddots & \ddots & 0 \\ & & 0 & 1 & -2 & 1 \\ & & & 0 & 1 & -2 \end{pmatrix}, \text{ is } M \times M.$$

Appendix B. Discrete Hamiltonians For The Timsohenko Schemes

Section 3.5 contains the sufficient and necessary conditions for the non-negativity of the discrete Hamiltonians. Here the Hamiltonians are derived, and conditions on their non-negativity are discussed. Before proceeding, it is worth introducing some notation, along with some useful identities. Summation by parts and related techniques are borrowed from [32, 33], and appear as well in [31]. The definitions of the finite difference operators are given in Table 2.

Appendix B.1. Discrete Inner Product And Norm

Much as for the continuous case in Section 2.4, for two grid functions f_m, g_m, where $m \in \mathbb{M} \triangleq [0, \ldots, M]$, it is possible to define an inner product and associated norm, in the following way

$$\langle f, g \rangle_{\mathbb{M}} \triangleq \sum_{m=0}^{M} h f_m g_m, \qquad \|f\|^2_{\mathbb{M}} \triangleq \langle f, f \rangle_{\mathbb{M}} \,. \tag{B.1}$$

In the following, other subdomains of $\mathbb{M}$, lacking at least one end point, will be used. These are

$$\underline{\mathbb{M}} \triangleq [0 : M-1], \quad \overline{\mathbb{M}} \triangleq [1 : M], \quad \underline{\overline{\mathbb{M}}} \triangleq [1 : M-1]$$

Appendix B.2. Identities And Summation By Parts

The following identities hold for generic grid functions f^n_m, g^n_m, and can be verified easily by direct calculation.

$$(\delta_{tt} f^n_m)\,(\delta_{t\cdot} f^n_m) = \delta_{t+} \frac{(\delta_{t-} f^n_m)^2}{2} \tag{B.2a}$$

$$(\mu_{tt} f^n_m)\,(\delta_{t\cdot} f^n_m) = \delta_{t+} \frac{(\mu_{t-} f^n_m)^2}{2} \tag{B.2b}$$

$$f^n_m\,(\delta_{t\cdot} f^n_m) = \delta_{t+} \frac{(f^n_m\, e_{t-} f^n_m)}{2} \tag{B.2c}$$

$$(f^n_m\, e_{t-} f^n_m) = (\mu_{t-} f^n_m)^2 - \frac{k^2}{4} (\delta_{t-} f^n_m)^2 \tag{B.2d}$$

Another useful identity involves summation by parts, and the spatial difference operators. This is given as

$$\begin{aligned} \langle \delta_{xx} f^n, g^n \rangle_{\mathbb{M}} &= -\langle \delta_{x+} f^n, \delta_{x+} g^n \rangle_{\underline{\mathbb{M}}} + (\delta_{x+} f^n_M) g^n_M - (\delta_{x-} f^n_0) g^n_0 \\ &= -\langle \delta_{x-} f^n, \delta_{x-} g^n \rangle_{\overline{\mathbb{M}}} + (\delta_{x+} f^n_M) g^n_M - (\delta_{x-} f^n_0) g^n_0 \end{aligned} \tag{B.3}$$

Appendix B.3. Discrete Hamiltonian For The Second-Order Accurate Scheme

An inner product of (15a) with $\delta_{t\cdot} w^n$ is taken over $\mathbb{M}$. This gives

$$\langle \delta_{tt} w^n, \delta_{t\cdot} w^n \rangle_{\mathbb{M}} = (\alpha - 1) \langle \delta_{xx} w^n, \delta_{t\cdot} w^n \rangle_{\mathbb{M}} + \langle \delta_{xx} w^n - \delta_{x-} \phi^n, \delta_{t\cdot} w^n_m \rangle_{\mathbb{M}}$$

Using identities (B.2a), (B.2c), (B.3) and end conditions (16), one gets from the above

$$\begin{aligned} \delta_{t+} \left(\frac{\|\delta_{t-} w^n\|^2_{\mathbb{M}}}{2} + \frac{(\alpha - 1) \left\langle \delta_{x+} w^n, \delta_{x+} w^{n-1} \right\rangle_{\underline{\mathbb{M}}}}{2} \right) = \\ - \left\langle \delta_{x+} w^n_m - \phi^n_{m+1/2}, \delta_{t\cdot} (\delta_{x+} w^n_m) \right\rangle_{\underline{\mathbb{M}}} + \mathfrak{b}_w \end{aligned} \tag{B.4}$$

Similarly, one takes an inner product of (15) with $\delta_{t\cdot} \phi^n$ over $\underline{\mathbb{M}}$, to get

$$\delta_{t+} \left(\frac{\|\delta_{t-} \phi^n\|^2_{\underline{\mathbb{M}}}}{2} + \frac{\beta \left\langle \delta_{x-} \phi^n, \delta_{x-} \phi^{n-1} \right\rangle_{\mathbb{M}}}{2} \right) = \left\langle \delta_{x+} w^n_m - \phi^n_{m+1/2}, \delta_{t\cdot} (\phi^n_{m+1/2}) \right\rangle_{\underline{\mathbb{M}}} + \mathfrak{b}_\phi \tag{B.5}$$

Adding (B.4) and (B.5), and using (B.2b) gives

$$\delta_{t+} \mathfrak{h}^{n-1/2}_{(2)} = \mathfrak{b}_w + \mathfrak{b}_\phi, \tag{B.6}$$

where

$$\mathfrak{h}_{(2)}^{n-1/2} = \frac{\|\delta_{t-} w^n\|_{\mathbb{M}}^2}{2} + \frac{\|\delta_{t-} \phi^n\|_{\underline{\mathbb{M}}}^2}{2} + \frac{(\alpha-1)\left\langle \delta_{x+} w^n, \delta_{x+} w^{n-1}\right\rangle_{\underline{\mathbb{M}}}}{2} + \frac{\beta\left\langle \delta_{x-} \phi^n, \delta_{x-} \phi^{n-1}\right\rangle_{\mathbb{M}}}{2} + \frac{\left\langle (\delta_{x+} w^n - \phi^n), (\delta_{x+} w^{n-1} - \phi^{n-1})\right\rangle_{\underline{\mathbb{M}}}}{2} \tag{B.7}$$

and where $\mathfrak{b}_w$, $\mathfrak{b}_\phi$ are boundary terms of the form

$$\begin{aligned} \mathfrak{b}_w &= (\alpha\delta_{x+} w_M^n - \phi_{M-1/2}^n)\delta_{t\cdot} w_M^n - (\alpha\delta_{x-} w_0^n - \phi_{-1/2}^n)\delta_{t\cdot} w_0^n \\ \mathfrak{b}_\phi &= \beta(\delta_{x+}\phi_{M-1/2})(\delta_{t\cdot}\phi_{M-1/2}) - \beta(\delta_{x-}\phi_{1/2})(\delta_{t\cdot}\phi_{1/2}) \end{aligned} \tag{B.8}$$

Clearly $\mathfrak{h}^{n-1/2}$ is the discrete counterpart to (11), and the boundary terms vanish under numerical simply-supported conditions (16).

Owing to (B.2d), the Hamiltonian may be bounded from below, as

$$2\mathfrak{h}_{(2)}^{n-1/2} \geq \|\delta_{t-} w^n\|_{\mathbb{M}}^2 + \|\delta_{t-}\phi^n\|_{\underline{\mathbb{M}}}^2 - \frac{(\alpha-1)k^2}{4}\|\delta_{x+}\delta_{t-} w^n\|_{\underline{\mathbb{M}}}^2 - \frac{\beta k^2}{4}\|\delta_{x-}\delta_{t-}\phi^n\|_{\mathbb{M}}^2 - \frac{k^2}{4}\|(\delta_{x+}\delta_{t-} w^n - \delta_{t-}\phi^n)\|_{\underline{\mathbb{M}}}^2 \triangleq \mathfrak{g}_{(2)}^{n-1/2} \tag{B.9}$$

By expanding out the last term, and after summation by parts under the choice of the simply supported numerical end conditions (16), this bound may be expressed as

$$\mathfrak{g}_{(2)}^{n-1/2} = \|\delta_{t-} w^n\|_{\overline{\mathbb{M}}}^2 + \left(1 - \frac{k^2}{4}\right)\|\delta_{t-}\phi^n\|_{\underline{\mathbb{M}}}^2 + \frac{\alpha k^2}{4}\left\langle \delta_{t-} w^n, \delta_{xx}\delta_{t-} w^n\right\rangle_{\overline{\mathbb{M}}} + \frac{\beta k^2}{4}\left\langle \delta_{t-}\phi^n, \delta_{xx}\delta_{t-}\phi\right\rangle_{\mathbb{M}} + \frac{k^2}{4}\left\langle \delta_{x+}\delta_{t-} w^n, \delta_{t-}\phi^n\right\rangle_{\underline{\mathbb{M}}} - \frac{k^2}{4}\left\langle \delta_{t-} w^n, \delta_{x-}\delta_{t-}\phi^n\right\rangle_{\overline{\mathbb{M}}} \tag{B.10}$$

This bound is a quadratic form. Let

$$\mathbf{u}^{n-1/2} \triangleq {}^{\mathsf{T}}[\delta_{t-}\mathbf{w}^n,\ \delta_{t-}\boldsymbol{\phi}^n]$$

then

$$\mathfrak{g}_{(2)}^{n-1/2} = {}^{\mathsf{T}}(\mathbf{u}^{n-1/2})\mathbf{G}_{(2)}\ \mathbf{u}^{n-1/2}$$

where $\mathbf{G}_{(2)}$ is a time-independent block matrix, of the form

$$\mathbf{G}_{(2)} = \left[\begin{array}{c|c} \mathbf{1}^w + \alpha\frac{k^2}{4}\mathbf{D}_{xx}^w & -\frac{k^2}{4}\mathbf{D}_{x-}^\phi \\ \hline \frac{k^2}{4}\mathbf{D}_{x+}^w & \left(1 - \frac{k^2}{4}\right)\mathbf{1}^\phi + \beta\frac{k^2}{4}\mathbf{D}_{xx}^\phi \end{array}\right]. \tag{B.11}$$

A condition on the non-negativity of the eigenvalues of $\mathbf{G}_{(2)}$ will result in the non-negativity of the Hamiltonian $\mathfrak{h}_{(2)}^{n-1/2}$, for all n. Because the diagonal terms are symmetric, and the non-diagonal terms are the transpose of each other, one such condition may be extracted by assuring

$$\mathbf{1}^w + \alpha\frac{k^2}{4}\mathbf{D}_{xx}^w \geq 0 \tag{B.12a}$$

$$\left(1 - \frac{k^2}{4}\right)\mathbf{1}^\phi + \beta\frac{k^2}{4}\mathbf{D}_{xx}^\phi + \frac{k^4}{16}\mathbf{D}_{x+}^w\left[\mathbf{1}^\phi + \alpha\frac{k^2}{4}\mathbf{D}_{xx}^w\right]^{-1}\mathbf{D}_{x-}^\phi \geq 0 \tag{B.12b}$$

Because the matrix $\mathbf{D}_{xx}^{w}$ is negative definite, and bounded from below by $-4/h^2$, one may go on and extract the following conditions for k and h.

$$k^2 \leq 4 \tag{B.13a}$$

$$h^2 \geq \frac{-B+\sqrt{\Delta}}{2A} \tag{B.13b}$$

where

$$A=(4-k^2),\ B=k^4(\alpha-1)-4k^2(\alpha+\beta),\ C=4\alpha\beta k^4,\ \Delta=B^2-4AC$$

Appendix B.4. Discrete Hamiltonian For The Fourth-Order Accurate Scheme

Taking again an inner product of $\delta_{t\cdot}w^n$ with (17a), and of $\delta_{t\cdot}\phi^n$ with (17b), using the same energetic manipulations as for the second-order accurate scheme, it is possible to show that a discrete Hamiltonian associated with the fourth-order accurate scheme is

$$\begin{aligned}\mathfrak{h}_{(4)}^{n-1/2}=\mathfrak{h}_{(2)}^{n-1/2}&-\frac{(1-\theta_1)h^2}{2}\frac{\|\delta_{t-}\delta_{x+}w^n\|_{\mathbb{M}}^2}{2}-\frac{(\alpha-1)(1-\theta_2)h^2}{2}\frac{\left\langle\delta_{xx}w^n,\delta_{xx}w^{n-1}\right\rangle_{\mathbb{M}}}{2}\\&+\frac{(1-\theta_3)h^2}{2}\frac{\|\delta_{x+}\delta_{t-}w^n-\delta_{t-}\phi^n\|_{\mathbb{M}}^2}{2}+\frac{(1-\theta_4)h^2}{2}\frac{\|\delta_{t-}\phi^n\|_{\mathbb{M}}^2}{2}\\&-\frac{(1-\theta_5)h^2}{2}\frac{\left\langle\delta_{x-}\phi^n,\delta_{x-}\phi^{n-1}\right\rangle_{\mathbb{M}}}{2}\end{aligned} \tag{B.14}$$

where $\mathfrak{h}_{(2)}^{n-1/2}$ is given by (B.19)

By means of (B.2d), the discrete Hamiltonian can be bounded from below, giving

$$\begin{aligned}2\mathfrak{h}_{(4)}^{n-1/2}\geq\mathfrak{g}_{(2)}^{n-1/2}&-\frac{(1-\theta_1)h^2}{2}\|\delta_{t-}\delta_{x+}w^n\|_{\mathbb{M}}^2+\frac{(\alpha-1)(1-\theta_2)h^2k^2}{8}\|\delta_{t-}\delta_{xx}w^n\|_{\mathbb{M}}^2\\&+\frac{(1-\theta_3)h^2}{2}\|\delta_{x+}\delta_{t-}w^n-\delta_{t-}\phi^n\|_{\mathbb{M}}^2+\frac{(1-\theta_4)h^2}{2}\|\delta_{t-}\phi^n\|_{\mathbb{M}}^2\\&+\frac{(1-\theta_5)h^2k^2}{8}\|\delta_{t-}\delta_{x-}\phi^n\|_{\mathbb{M}}^2\triangleq\mathfrak{g}_{(4)}^{n-1/2}\end{aligned} \tag{B.15}$$

where $\mathfrak{g}_{(2)}^{n-1/2}$ is given in (B.10). Using again summation by parts, under the choice of numerical boundary conditions (16) and (20), one may write down $\mathfrak{g}_{(4)}^{n-1/2}$ as a quadratic form, in the same way that (B.9) was ported to the form (B.10).

Thus, let again

$$\mathbf{u}^{n-1/2}\triangleq{}^{\mathsf{T}}[\delta_{t-}\mathbf{w}^n,\ \delta_{t-}\boldsymbol{\phi}^n]$$

then

$$\mathfrak{g}_{(4)}^{n-1/2}={}^{\mathsf{T}}(\mathbf{u}^{n-1/2})\mathbf{G}_{(4)}\ \mathbf{u}^{n-1/2}$$

where $\mathbf{G}_{(4)}$ is a time-independent block matrix, of the form

$$\mathbf{G}_{(4)}=\left[\begin{array}{c|c}\mathbf{A}_{(4)}&\mathbf{B}_{(4)}\\\hline{}^{\mathsf{T}}\mathbf{B}_{(4)}&\mathbf{C}_{(4)}\end{array}\right].$$

where

$$\mathbf{A}_{(4)} = \mathbf{1}^w + \left[\frac{(1-\theta_1)h^2}{2} + \frac{k^2}{4}(\alpha - 2(1-\theta_3))\right]\mathbf{D}^w_{xx} + \frac{(\alpha-1)(1-\theta_2)h^2k^2}{8}\mathbf{D}^w_{xxxx} \tag{B.16a}$$

$$\mathbf{B}_{(4)} = \left[\frac{k^2}{4} - \frac{(1-\theta_3)k^2}{2}\right]\mathbf{D}^\phi_{x-} \tag{B.16b}$$

$$\mathbf{C}_{(4)} = \left[1 + \frac{(1-\theta_4)h^2}{2} + \frac{k^2}{4}(1-2\theta_3)\right]\mathbf{1}^\phi + \frac{k^2}{4}\left[\beta - \frac{(1-\theta_5)h^2}{2}\right]\mathbf{D}^\phi_{xx} \tag{B.16c}$$

This is a generalised form for the Hamiltonian, depending on the five free parameters. Notice that, as expected, this form reduces to (B.11) when $\theta_i = 1$ for all i. From block matrix theory, $\mathbf{G}_{(4)}$ is positive definite if and only if

$$\mathbf{A}_{(4)} > 0 \tag{B.17a}$$

$$\mathbf{C}_{(4)} - {}^{\mathsf{T}}\mathbf{B}_{(4)}\mathbf{A}^{-1}_{(4)}\mathbf{B}_{(4)} \geq 0 \tag{B.17b}$$

It is possible to show that the above condition are equivalent to

$$\mathbf{A}_{(4)} > 0 \tag{B.18a}$$

$$\beta - \frac{(1-\theta_5)h^2}{2} \geq 0 \tag{B.18b}$$

$$1 + \frac{(1-\theta_4)h^2}{2} + \frac{k^2}{4}(1-2\theta_3) - \frac{k^2}{h^2}\left(\beta - \frac{(1-\theta_5)h^2}{2}\right) - \frac{4}{h^2\lambda^{(min)}_{\mathbf{A}_{(4)}}}\left(\frac{k^2}{4} - \frac{(1-\theta_3)k^2}{2}\right)^2 \geq 0 \tag{B.18c}$$

Equation (B.18c) corresponds to condition (B.17b), under the assumptions that $\mathbf{A}_{(4)} > 0$ and that, in (B.16c), the matrix $\left[\beta - \frac{(1-\theta_5)h^2}{2}\right]\mathbf{D}^\phi_{xx}$ is negative definite, and hence bounded from below. Notice that the left hand side of (B.18c) is a cubic polinomial in h^2, whose roots can only be found via an iterative root finding algorithm (such as Newton-Raphson).

Appendix B.5. Discrete Hamiltonan For The Wideband Accurate Scheme

Taking again an inner product of $\delta_{t\cdot}w^n$ with (21a), and of $\delta_{t\cdot}\phi^n$ with (21b), using the same energetic manipulations as for the second-order accurate scheme, it is possible to show that a discrete Hamiltonian associated with the fourth-order accurate scheme is

$$\begin{aligned}\mathfrak{h}^{n-1/2}_{(W)} = {} & \frac{\|\delta_{t-}w^n\|^2_{\mathbb{M}}}{2} + \frac{\|\delta_{t-}\phi^n\|^2_{\mathbb{M}}}{2} + \frac{h^2(\theta-1)\|\delta_{t-}\delta_{x+}w^n\|^2_{\mathbb{M}}}{4} + \frac{h^2(\theta-1)\|\delta_{t-}\delta_{x-}\phi^n\|^2_{\mathbb{M}}}{4} \\ & + \frac{(\alpha-1)\left\langle\delta_{x+}w^n, \delta_{x+}w^{n-1}\right\rangle_{\mathbb{M}}}{2} + \frac{\beta\|\mu_{t-}(\delta_{x-}\phi^n)\|^2_{\mathbb{M}}}{2} + \frac{\|\mu_{t-}(\delta_{x+}w^n - \phi^n)\|^2_{\mathbb{M}}}{2}\end{aligned} \tag{B.19}$$

By means of (B.2d), and using integration by parts under end conditions (16), the Hamiltonian can be bounded from below, as

$$\begin{aligned}2\mathfrak{h}^{n-1/2}_{(W)} \geq {} & \|\delta_{t-}w^n\|^2_{\mathbb{M}} + \|\delta_{t-}\phi^n\|^2_{\mathbb{M}} - \frac{(\alpha-1)k^2}{4}\left\langle\delta_{t-}w^n, \delta_{xx}\delta_{t-}w^n\right\rangle^2_{\mathbb{M}} \\ & - \frac{h^2(\theta-1)\left\langle\delta_{t-}w^n, \delta_{t-}\delta_{xx}w^n\right\rangle^2_{\mathbb{M}}}{2} - \frac{h^2(\theta-1)\left\langle\delta_{t-}\phi^n, \delta_{t-}\delta_{xx}\phi^n\right\rangle^2_{\mathbb{M}}}{2} \triangleq \mathfrak{g}^{n-1/2}_{(W)}\end{aligned} \tag{B.20}$$

where $\mathfrak{g}_{(W)}^{n-1/2}$ can be written as a quadratic form. Thus, let again

$$\mathbf{u}^{n-1/2} \triangleq \mathsf{T}[\delta_{t-}\mathbf{w}^n,\ \delta_{t-}\boldsymbol{\phi}^n]$$

then

$$\mathfrak{g}_{(W)}^{n-1/2} = \mathsf{T}(\mathbf{u}^{n-1/2})\mathbf{G}_{(W)}\ \mathbf{u}^{n-1/2}$$

where $\mathbf{G}_{(W)}$ is a time-independent block matrix, of the form

$$\mathbf{G}_{(W)} = \left[\begin{array}{c|c} \mathbf{1}^w - \left(\frac{(\alpha-1)k^2}{4} + \frac{(\theta-1)h^2}{2}\right)\mathbf{D}_{xx}^w & \mathbf{0}^\phi \\ \hline \mathbf{0}^w & \mathbf{1}^\phi - \frac{(\theta-1)h^2}{2}\mathbf{D}_{xx}^\phi \end{array}\right]. \tag{B.21}$$

which is positive-definite if and only if

$$\theta > \frac{1}{2} \tag{B.22a}$$

$$h^2 \geq \frac{(\alpha-1)k^2}{2\theta-1} \tag{B.22b}$$